Spectroscopy above the ionization threshold: Dissociative recombination of the ground vibrational level of N_2^+

Steven L. Guberman[a)]
Institute for Scientific Research, 22 Bonad Road, Winchester, Massachusetts 01890, USA

(Received 22 May 2012; accepted 12 July 2012; published online 21 August 2012)

Comprehensive theoretical calculations are reported for the dissociative recombination of the lowest vibrational level of the N_2^+ ground state. Fourteen dissociative channels, 21 electron capture channels, and 48 Rydberg series including Rydberg states having the first excited state of the ion as core are described for electron energies up to 1.0 eV. The calculation of potential curves, electron capture and predissociation widths, cross sections and rate constants are described. The cross sections and rate constants are calculated using Multichannel Quantum Defect Theory which allows for efficient handling of the Rydberg series. The most important dissociative channel is $2^3\Pi_u$ followed by $4^3\Pi_u$. Dissociative states that do not cross the ion within the ground vibrational level turning points play a significant role in determining the cross section structure and at isolated energies can be more important than states having a favorable crossing. By accounting for autoionization, the interactions between resonances, between dissociative states, and between resonances and dissociative states it is found that the cross section can be viewed as a complex dissociative recombination spectrum in which resonances overlap and interfere. The detailed cross section exhibits a rapid variation in atomic quantum yields for small changes in the electron energy. A study of this rapid variation by future high resolution storage ring experiments is suggested. A least squares fit to the calculated rate constant from the ground vibrational level is $2.2^{+0.2}_{-0.4} \times 10^{-7} \times (T_e/300)^{-0.40}$ cm^3/ sec for electron temperatures, T_e, between 100 and 3000 K and is in excellent agreement with experimentally derived values. © *2012 American Institute of Physics*. [http://dx.doi.org/10.1063/1.4739472]

I. INTRODUCTION

The dissociative recombination (DR) of N_2^+,

$$N_2^+ + e^- \rightarrow N + N, \quad (1)$$

where e^- is an electron and the N atoms may be electronically excited was first discussed 66 years ago in a review of reactions in the Earth's ionosphere[1] and shortly thereafter in an analysis of the characteristics of an N_2 discharge afterglow[2,3] and a microwave afterglow.[4] In the interim, it has been the subject of microwave afterglow,[5–12] shock tube,[13] merged beam,[14,15] and storage ring[16,17] experiments. It is also well recognized as an important process in the ionospheres of Earth,[18,19] Mars,[20] Titan,[21] and Triton.[22] While aspects of several channels that contribute to the DR of N_2^+ have been reported previously,[23–26] this is the first comprehensive report of the calculation of total and partial DR cross sections and rate constants for N_2^+ over both major and minor dissociative routes. The role of minor dissociative routes (i.e., routes that do not cross within the $v = 0$ turning points or have very small capture widths) has not been adequately explored in prior theoretical studies and it is especially crucial if one is to compare *ab initio* cross sections to those derived from future vibrationally resolved high resolution storage ring experiments. In addition, minor routes for DR of $v = 0$ may be major routes for DR of $v > 0$ levels and the work reported here will set the foundation for the study of the DR of excited levels. The latter will be reported separately.

A schematic depiction of DR is shown in Fig. 1. In direct recombination,[27] an electron with energy ε is captured by a molecular ion into a dissociative state in which autoionization can also occur. If the neutral state crosses the ion within the vibrational turning points, the Franck-Condon factor between the ion and neutral state vibrational wave functions will be large. Capture is also driven by an electronic width. If the magnitude of the width is favorable, the DR cross section for the direct process will be large. If the electronic width is too small, the electron will have a low probability of capture and if it is too large the electron may be ejected before dissociation. Once the internuclear distance increases beyond the crossing point of the ion and dissociative state, the probability of autoionization becomes small and the capture is complete, leading to a high rate compared to that for electron capture by atomic ions. The electronic capture width is usually due to two electron interactions. However, it has been shown that direct capture can take place by an interaction of the incoming electron with the nuclear motion.[28,29]

Neutral, vibrationally excited ground core Rydberg states are present in the electron-ion continuum. In indirect recombination,[30] the electron (with energy ε' in Fig. 1) is captured into a vibrationally excited neutral Rydberg state by interaction between the electron motion and the nuclear motion (Born-Oppenheimer break down). This is followed by predissociation along the same neutral repulsive state of the direct

a)slg@sci.org.

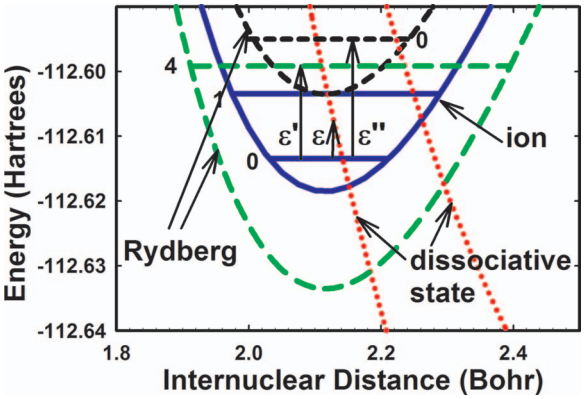

FIG. 1. Schematic representation of DR. The ground state of the ion (solid blue line) and the lowest two vibrational levels are shown with two dissociative states (red dots). Also shown is a Rydberg state having the ion ground state as core (long green dashes) and a core excited Rydberg state (short black dashes).

mechanism or by autoionization. The interference between direct and indirect recombination must be accounted for and is included in the calculated cross sections and rate coefficients described below.

In an additional second order mechanism[31–33] included in the calculations described below, the neutral repulsive state acts as an intermediate between the electron-ion and a bound Rydberg state. In this manner, an electron can be first captured by an electron-electron interaction into a repulsive state followed by another electron-electron interaction connecting to the Rydberg state.

The Rydberg states can also act as intermediaries and can couple together repulsive states of the same symmetry allowing for electron capture into one repulsive state followed by partial dissociation along another state.[34,35] This mechanism is especially important for N_2^+.

Capture into excited core Rydberg states[24,36–38] is also an important mechanism for N_2^+ DR. For these states, capture can take place by an electronic mechanism as opposed to the first order Born-Oppenheimer break down coupling and the second order electronic coupling needed to have capture into a Rydberg state with a ground state core. This coupling can often be much larger than the Born-Oppenheimer breakdown or second order couplings. In addition, capture can occur into the v = 0 level of an excited core Rydberg state. This is not possible for ground state core Rydberg states since the v = 0 level lies below the ion v = 0 level. If the core excited Rydberg state potential curve is nearly parallel to the ground state ion curve, large Franck-Condon factors for capture are possible. This mechanism was first described[37] in calculations done in this laboratory on the DR of N_2^+.

Spin-orbit coupling between Rydberg states[39,40] can also play an important role in DR. However, due to the Σ symmetry of the N_2^+ ground state, it does not play a role in N_2^+ DR.

All of these mechanisms are included and allowed to interfere in the Multichannel Quantum Defect Theory (MQDT) approach used here.

The *ab initio* description of DR presented here requires accurate potential curves for the description of the ion and the neutral states. In Sec. II, the calculation of the potential curves is described and the important states which drive DR are identified. The electronic capture widths and quantum defects are discussed in Sec. III. The details of the cross section calculations including a discussion of the contributions of the various dissociative states can be found in Sec. IV. Section V has the rate coefficients and comparisons to experimentally derived values. Conclusions are in Sec. VI.

II. POTENTIAL CURVES

The valence states of the atoms that can arise from DR of the v = 0 level of the ion ground state with a zero energy electron are (with the total released kinetic energy):

$$N_2^+ + e^- \rightarrow N(^4S) + N(^4S) \quad (5.822\ \text{eV}), \tag{2a}$$

$$N_2^+ + e^- \rightarrow N(^4S) + N(^2D) \quad (3.438\ \text{eV}), \tag{2b}$$

$$N_2^+ + e^- \rightarrow N(^4S) + N(^2P) \quad (2.246\ \text{eV}), \tag{2c}$$

$$N_2^+ + e^- \rightarrow N(^2D) + N(^2D) \quad (1.055\ \text{eV}), \tag{2d}$$

$$N_2^+ + e^- \rightarrow N(^2P) + N(^2D) \quad (-0.137\ \text{eV}), \tag{2e}$$

and

$$N_2^+ + e^- \rightarrow N(^2P) + N(^2P) \quad (-1.328\ \text{eV}). \tag{2f}$$

For channels (2e) and (2f), DR is not possible from v = 0 unless the electron energy exceeds 0.137 eV and 1.328 eV, respectively. For v = 1, DR is energetically possible with a zero energy electron for channel (2e). DR along Channel (2f) is exothermic at v = 6 for a zero energy electron.

102 molecular states arise from the atomic asymptotes in (2a)–(2f). For the $^2\Sigma_g^+$ ion ground state, possible dissociative states must be of singlet or triplet spin symmetry and cannot have minus symmetry. Eliminating Γ and Φ states (since they are likely to have very small electron capture widths) reduces the total number of possible dissociative states to 64 with 12 possible symmetries: $^{1,3}\Sigma_{g,u}^+$, $^{1,3}\Pi_{g,u}$, and $^{1,3}\Delta_{g,u}$.

In studies of the DR of diatomics, it is often necessary to use diabatic states, i.e., states that have the ion ground state (or Rydberg character) projected out of the wave function. Fully optimized dissociative states without this projection have avoided crossings with Rydberg states and cannot cross the ion. In the case of H_2, the projection can be done exactly by simply removing the $1\sigma_g$ orbital from the configuration interaction wave function. For larger diatomics, an approximate projection operator can be applied by using only valence basis sets devoid of Rydberg basis functions. This approach has been recognized previously for N_2 by Stahel *et al.*:[41] "While the adiabatic electronic energies … represent the aim of accurate quantum chemical calculations,[42] the results achieved by excluding Rydberg-type orbitals[43] correspond closely to the diabatic valence states $b'^1\Sigma_u^+$ and $b^1\Pi_u$." Because of the removal of Rydberg character, the spectroscopic constants of the diabatic wave functions do not always

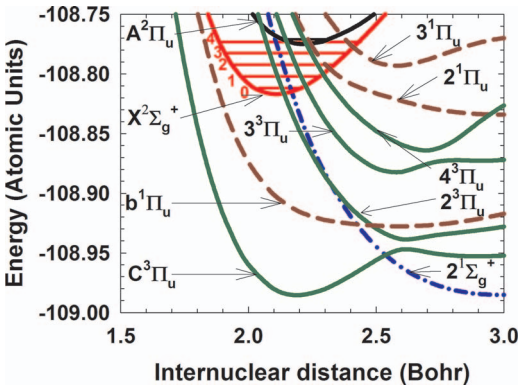

FIG. 2. Adiabatic $^3\Pi_u$, $^1\Pi_u$ and $^1\Sigma_g^+$ states shown with the ion ground state and the lowest five vibrational levels. Also shown is the $A^2\Pi_u$ ion with the v = 0 vibrational level.

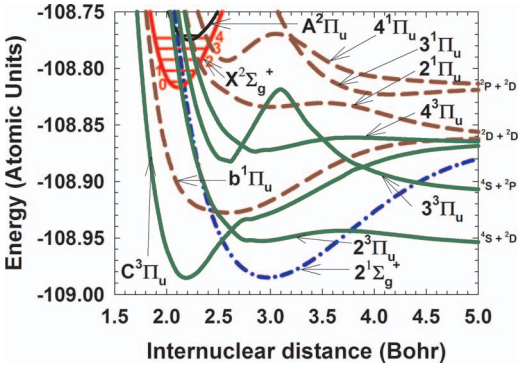

FIG. 3. Same as Fig. 2 except the $^3\Pi_u$ curves are shown as valence diabatic states and the abscissa is wider to show the dissociation limits.

compare well with experimentally derived values. Nevertheless, these comparisons are useful and are discussed below.

Large scale calculations in the 12 electronic symmetries are reported here. For all of the states, complete active space self consistent field (CASSCF) wave functions are used for determining the orbitals. In these calculations, the 2σ orbitals are active. The configuration interaction (CI) wave functions were constructed by taking all single and double excitations from a reference set which included the full CASSCF wave function. The $^3\Pi_u$ and $2^1\Sigma_g^+$ calculations use a [4s, 3p, 2d, 1f] (Ref. 44) basis set of contracted Gaussians based upon (13s, 8p) (Ref. 45) and (6d, 4f) (Ref. 44) primitive sets. The direct CI approach as implemented in MOLECULE-SWEDEN programs[46–48] is used. All other CASSCF (Ref. 49) and multireference configuration interaction (MRCI) (Ref. 50) calculations (with the internally contracted approach) are done with the MOLPRO programs.[51] For the $^1\Pi_u$ states, the cc-pVTZ (Ref. 52) basis is used. $^3\Delta_u$ and $^3\Sigma_u^+$ are expressed in a [4s, 3p, 3s, 2d, 1f] truncation of a [5s, 4p, 3s, 2d, 1f] (Ref. 52) contracted Gaussian set (cc-pVQZ (Ref. 52)) on each atom. This is described further below. The $b'^1\Sigma_u^+$, $w^1\Delta_u$, $^3\Delta_g$, $^3\Pi_g$, $^1\Pi_g$, $^3\Sigma_g^+$, $^1\Delta_g$, $^1\Sigma_g^-$, and $^1\Gamma_g$ calculations are done with the cc-pVQZ (Ref. 52) basis. All approaches include the Davidson correction to the CI energies. All calculations are in the D_{2h} point group. The π_{ux} and π_{uy} orbitals are forced to be equivalent as are π_{gx} and π_{gy}.

Potential curves which intersect the ion within the turning points of the v ≤ 4 vibrational levels are shown in Figs. 2, 3, 5, and 6. It is clear that states of the following symmetries may be major routes for the DR of the v = 0 level: $2^3\Pi_u$, $2\,^1\Sigma_g^+$, $G^3\Delta_g$, and $b'^1\Sigma_u^+$. The remaining minor routes (that cross the ion within the turning points of v = 1–4) are 3, $4^3\Pi_u$, 2, $3^1\Pi_u$, $2\,^3\Sigma_u^+$, $^3\Sigma_g^+$, $2^3\Delta_g$, $2^3\Pi_g$, and $1 - 3^1\Delta_g$.

A. $X^2\Sigma_g^+$ and $A^2\Pi_u$

The $X^2\Sigma_g^+$ ion curve consists of the Rydberg–Klein–Rees (RKR) (Ref. 60) points near the minimum and is supplemented at short and large R by calculated points. The calculated points have been reported previously.[24] The minimum of the ion curve is placed at the experimental R_e and at the experimental[60] T_e above the $X^1\Sigma_g^+$ ground state calculated with the same basis set and approach as the dissociative state of interest. For $A^2\Pi_u$, the cc-pVQZ (Ref. 52) basis set is used with the CASSCF and MRCI approach described above. The calculated value for R_e is 2.2261 a_o, 0.0083 a_o larger than the experimental[60] value. In the plots and in the DR calculations, the calculated curve is shifted to shorter R by 0.0083 a_o and placed at the experimental excitation energy above $X^2\Sigma_g^+$. The calculated values for ω_e and $\omega_e x_e$ differ from experiment[60] by 6 cm^{-1} and 0.1 cm^{-1}, respectively. The shifted curve has been reported previously.[24]

B. Π_u states

All curves in Figs. 2 and 3 are calculated in the [4s, 3p, 2d, 1f] or the cc-pVTZ basis using either the direct CI or internally contracted approach. The calculated potential points are in Table I for the $^3\Pi_u$ states. For the $^3\Pi_u$ and $^1\Pi_u$ states, the CASSCF orbitals were determined by averaging over the lowest five roots. In the CASSCF and CI calculations for $^3\Pi_u$ ($^1\Pi_u$), one of the five roots is $^3\Phi_u$ ($^1\Phi_u$).

Although all the curves in the Figures are diabatic in the sense that they omit Rydberg character, the $^3\Pi_u$ potential curves used in the cross section calculations are also diabatic since they are allowed to cross. Landau-Zener calculations[53] of the crossing probabilities show that the diabatic paths in Fig. 3 are much more likely to be followed than the adiabatic paths in Fig. 2. The diabatic potential curves were obtained by simply interchanging the adiabatic points. A more rigorous adiabatic-diabatic transformation is expected to have a negligible effect upon the calculated DR cross sections and rate coefficients. Table I has the calculated diabatic $^3\Pi_u$ curves. Figures 2 and 3 show that $2^3\Pi_u$, $3^3\Pi_u$, and $4^3\Pi_u$ cross the ion ground state between the v = 0, 1, 2 turning points, respectively. $C^3\Pi_u$ does not cross the ion. $2^1\Pi_u$ crosses between the v = 2 turning points and $3^1\Pi_u$ crosses near the outer turning point of v = 3. Of the Π_u states, only the diabatic $2^3\Pi_u$ state goes to the $N(^4S) + N(^2D)$ limit. The $3^3\Pi_u$ diabatic state goes to the $N(^4S) + N(^2P)$ limit. The remaining Π_u states go to the $N(^2D) + N(^2D)$ with the exception of $3^1\Pi_u$ which dissociates to $N(^2P) + N(^2D)$.

TABLE I. Energies (a.u.) for the $^3\Pi_u$ potential curves.[a]

R(a_o)	$C^3\Pi_u$	$C'^3\Pi_u$	$3^3\Pi_u$	$4^3\Pi_u$
1.75	−0.792562			
1.8	−0.844214			
1.85	−0.885277			
1.9	−0.917341	−0.616353	−0.559049	−0.533829
1.95	−0.941767			
2.0	−0.959731	−0.718772	−0.665681	−0.634088
2.1	−0.980190	−0.793656	−0.743598	−0.709181
2.2	−0.985330	−0.847605	−0.799662	−0.763692
2.3	−0.980244	−0.885792	−0.838901	−0.802546
2.4	−0.969138	−0.912140	−0.864766	−0.829613
2.5	−0.956118	−0.929507	−0.879089	−0.847834
2.6			−0.882118	−0.859338
2.649			−0.879232	
2.7	−0.936325	−0.949364		
2.8	−0.933541	−0.952067	−0.856765	−0.872379
2.9	−0.931037	−0.952857	−0.840924	−0.872761
3	−0.928005	−0.952256	−0.826456	−0.872064
3.1	−0.924275	−0.950839	−0.818573	−0.870482
3.2	−0.919776	−0.949040	−0.827500	−0.868469
3.3	−0.915012	−0.947237	−0.841348	−0.866342
3.4	−0.910021	−0.945679	−0.853050	−0.864443
3.5	−0.904980	−0.944522		
3.6	−0.900044	−0.943841	−0.870895	−0.861839
3.7	−0.895264	−0.943636	−0.878352	−0.861361
3.8	−0.889962	−0.943855	−0.883907	−0.861245
3.9	−0.887035	−0.944416	−0.887515	−0.861378
4	−0.883597	−0.945223	−0.891242	−0.861655
4.2	−0.878085	−0.947222	−0.896949	−0.862383
4.4	−0.874221	−0.949291	−0.900922	−0.863123
4.6	−0.871580	−0.951127	−0.903705	−0.863767
4.8			−0.905659	−0.864284
5	−0.868537	−0.953764	−0.907030	−0.864679
5.2	−0.867667	−0.954610	−0.907987	−0.864964
5.4	−0.867051	−0.955215	−0.908648	−0.865162
5.6	−0.866616	−0.955637	−0.909099	−0.865289
5.8	−0.866305	−0.955922	−0.909403	−0.865368
6	−0.866076	−0.956109	−0.909601	−0.865412
6.2	−0.865903	−0.956228	−0.909726	−0.865429
6.4	−0.865771	−0.956299	−0.909800	−0.865427
6.6	−0.865670	−0.956339	−0.909841	−0.865414
6.8	−0.865591	−0.956357	−0.909860	−0.865395
7	−0.865528	−0.956362	−0.909864	−0.865372
7.2	−0.865479	−0.956360	−0.909860	−0.865347
7.4	−0.865439	−0.956352	−0.909852	−0.865323
7.6	−0.865408	−0.956343	−0.909841	−0.865301
7.8	−0.865382	−0.956332	−0.909829	−0.865282
8.0	−0.865361	−0.956322	−0.909817	−0.865264

[a]Add −108 to get the total energy.

Figure 2 shows an avoided crossing between the $C^3\Pi_u$ and $2^3\Pi_u$ curves near R = 2.5 a_o. Using spectroscopic data, the interaction matrix element, i.e., one-half the energy difference between the two states at the point of closest approach, was reported to be 700 cm^{-1}.[54] Recent determinations of the matrix element based upon additional spectroscopic data found values of 810 ± 20 cm^{-1} (Ref. 55) and 798 ± 15 cm^{-1} (Ref. 56) compared to theoretical estimates of 1000 cm^{-1} [55,57] and 770 cm^{-1}.[55] The value found here is 930 cm^{-1} and is in agreement with the prior values.

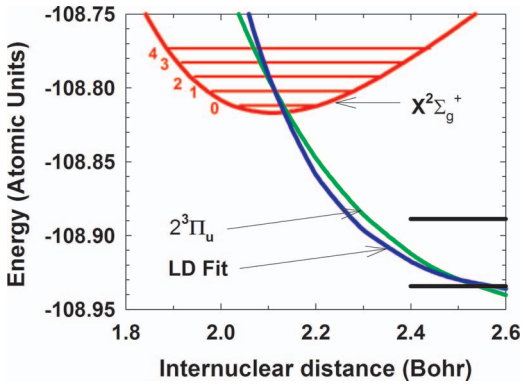

FIG. 4. Comparison of the calculated $2^3\Pi_u$ potential curve to the segment derived by Leoni and Dressler.[58]

Figure 4 shows a comparison of the $2^3\Pi_u$ curve of Figs. 2 and 3 with a segment of the curve derived from spectroscopic data by Leoni and Dressler,[58] $V(R) = 95516 + 123100\ R^{-12}$ cm^{-1} (with R in Angstroms). This segment has been plotted relative to v = 0 of the calculated $X^1\Sigma_g^+$ state (with the minimum at −109.38988 a.u.) in the [4s, 3p, 2d, 1f] direct CI approach. The black horizontal lines are the boundaries of the region (100 000–110 000 cm^{-1}) from which spectroscopic data was used to derive the segment. The $2^3\Pi_u$ curve matches the Leoni-Dressler fit near the lower boundary and deviates as the energy is increased. Near the ion, the deviation decreases and the calculated $2^3\Pi_u$ curve crosses the v = 0 level at an internuclear distance that is only 0.0053 a_o larger than the crossing point of the fit. However, the v = 0 level is about 20 000 cm^{-1} above the upper boundary and the accuracy of the fit near v = 0 is uncertain.

Calculated spectroscopic constants are compared to experiment[59,60] in Table II. $C'^3\Pi_u$ is the shallow outer well near 2.9 a_o in the adiabatic state labeled $C^3\Pi_u$ in Fig. 2 and the well in the $2^3\Pi_u$ state in Fig. 3. All the calculated spectroscopic values show a deviation from experiment that would be expected for the basis sets and wave functions used in this study with the exception of states with the broadest potential wells, i.e., the smallest ω_e's. These states, $b'^1\Sigma_u^+$, $b^1\Pi_u$, and $C'^3\Pi_u$, are in the same region as Rydberg states of the same symmetry and are known to have considerable Rydberg character.[42,61] The omission of Rydberg character in the basis set used here is the source of this disagreement. Had Rydberg character been included in the basis, it would become more important as R decreases leading to calculated R_e's that are smaller than those calculated here and in better agreement with the experimentally derived R_e's.

An alternative approach[62] to define diabatic states uses the matrix element of $\sum_i r_i^2$ where r_i is the distance between a nucleus and electron i. This approach requires the calculation of the adiabatic Rydberg states which is not done here (see below for the calculation of diabatic Rydberg states). The eigenvectors from the diagonalization of the property matrix over the adiabatic Rydberg and valence states are used to transform the adiabatic states to diabatic states. This approach has the advantage that diffuse character can mix into the valence state while preserving its overall valence character. It

TABLE II. Calculated spectroscopic values compared to experiment.[a]

	T_e (eV)		ω_e (cm^{-1})		$\omega_e x_e$ (cm^{-1})		R_e (a_o)	
	Calc.	Exp.	Calc.	Exp.	Calc.	Exp.	Calc.	Exp.
$^1\Phi_u$	13.961		704.8		17.73		2.958	
$H^3\Phi_u$	13.056	13.1077	903.3	924.21	13.25	12.29	2.846	2.8121
$b'^1\Sigma_u^{+\#}$	12.796	12.95	800.2	760.08	4.737	4.418	2.832	2.719
$b^1\Pi_u$	12.432	12.56	688	634.8	9.79		2.61	2.4266
$C'^3\Pi_u$	11.892	12.194	726	791	29.9	33.5	2.90	
$C^3\Pi_u$	11.007	11.05167#	1988	2047.17	24.97	28.445	2.193	2.1707
$2^1\Sigma_g^+$	11.02		933.8		2.978		2.975	
$2^3\Delta_g$	14.395		951.2		42.45		3.1975	
$G^3\Delta_g$	10.982	10.898	756.4	742.49	8.605	11.85	3.0575	3.0437
$w^1\Delta_u^{\#}$	8.827	8.939	1532	1559.496	11.67	12.0078	2.419	2.39774
$a^1\Pi_g$	8.547	8.590051	1703	1694.20	18.37	13.949	2.316	2.3060
$W^3\Delta_u$	7.347	7.4153	1505	1501	15.30	11.6	2.428	
$B^3\Pi_g$	7.348	7.39189	1729	1733.39	14.94	14.122	2.302	2.2915
$A^3\Sigma_u^+$	6.13	6.22449	1453	1460.64	16.4	13.87	2.44	2.4313

[a]All experimental values are from Ref. 59 except those with a # which are from Ref. 60.

would be interesting to compare the ion crossing points for the two methods. The calculated[62] T_e for $b^1\Pi_u$ is 12.610 eV with a recommended value of 12.470 eV in agreement with our calculated value of 12.432 eV. The calculated ω_e of 681.1 cm^{-1} and recommended value of 689.0 cm^{-1} are also in agreement with our value of 688 cm^{-1}. It should be noted that these values disagree with the purely experimental[59] value of 634.8 cm^{-1}. The reported[62] R_e of 2.46576 a_o is considerably smaller than our value of 2.61 a_o and is in closer agreement with the experimentally derived value of 2.4266 a_o.[59] For $b'^1\Sigma_u^+$, the recommended values for T_e and ω_e are 12.954 eV, 759.5 cm^{-1} and the calculated value for R_e is 2.73139 a_o compared to the values calculated here of 12.7957 eV, 800.2 cm^{-1}, and 2.832 a_o. A comparison to the experimentally derived values in Table II shows that the earlier values are in better agreement with experiment than those reported here indicating that the omission of Rydberg character has a larger effect upon the b′ state than the b state.

C. $b'^1\Sigma_u^+$ and $^1\Delta_u$

The $b'^1\Sigma_u^+$ potential curve crosses near the inner turning point of v = 0 as shown in Fig. 5 and leads to $N(^2P) + N(^2D)$ atoms which are not energetically accessible from v = 0 for electron energies below the experimental asymptote of 0.1374 eV. Above this threshold, this state may be important for DR of the ground level but it will not affect the room temperature rate constant. Below 0.1374 eV electron energy, DR along this route is energetically possible for excited vibrational levels. The $b'^1\Sigma_u^+$ potential curve is calculated in the cc-pVQZ basis.[52] The orbitals were determined for only the b′ state. b′ is the second root in a CASSCF in $^1B_{1u}$ symmetry of D_{2h}. The lowest root is $w^1\Delta_u$. Two roots are also calculated in the MRCI. Building upon a suggestion of Spelsberg and Meyer,[62] $4\sigma_g$, $4\sigma_u$, $2\pi_{gx}$, and $2\pi_{gy}$ are added to the active space with the restriction that they are singly occupied in the CASSCF and MRCI. For R ≤ 5.0 a_o, the w state is the lowest root and the b′ is the second CI root. For 5.0 ≤ R ≤ 7.0 a_o, four roots were obtained in the MRCI. The b′ state is the third root and the others are $^1\Delta_u$. For 7.2 a_o ≤ R ≤ 8.0 a_o, the b′ state is the second MRCI root.

$w^1\Delta_u$ is too low in energy to be of significance to DR. In addition, none of the Δ_u states will be important because in order for the $^2\Sigma_g^+$ ion to capture an electron into a Δ_u state, the electron must be in an f orbital (i.e., angular momentum quantum number, $\ell = 3$). In this case, the incoming electron has only a small overlap with the ion electrons and the electronic capture width will be very small.

D. $2^1\Sigma_g^+$

For $2^1\Sigma_g^+$, the orbitals are optimized for the second root in the CASSCF. Two roots are obtained in the CI. The calculation of the $2^1\Sigma_g^+$ curve has been reported previously,[24,63] where it was shown to be in good agreement although more accurate than two prior calculations.[64,65] Figures 2 and 3 show that the $2^1\Sigma_g^+$ potential curve crosses the ion between the v = 0 turning points and is a candidate for DR of v = 0.

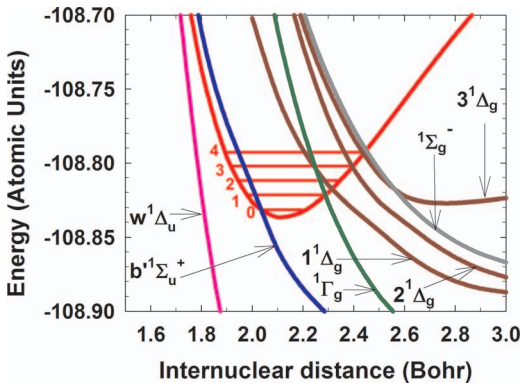

FIG. 5. The $b'^1\Sigma_u^+$, $^1\Delta_g$, $^1\Delta_u$, $^1\Sigma_g^-$ and $^1\Gamma_g$ dissociative states with the ion ground state.

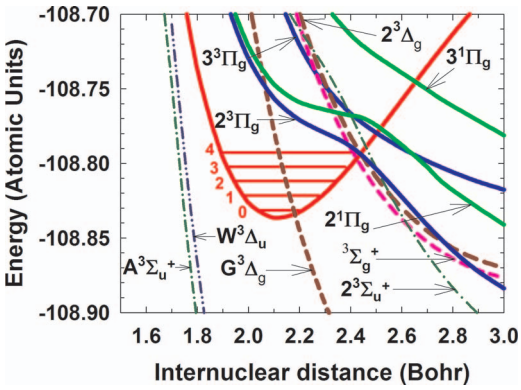

FIG. 6. The $^3\Delta_u$, $^3\Sigma_u^+$, $^3\Pi_g$, $^1\Pi_g$, $^3\Sigma_g^+$ and $^3\Delta_g$ dissociative states with the ion ground state. The $A^3\Sigma_u^+$, $W^3\Delta_u$ and $2^3\Sigma_u^+$ curves were shifted in energy in order to be shown with the ion which is at the experimental ionization potential above the ground state calculated in a cc-pVQZ basis (see Sec. II E).

E. $^3\Delta_u$ and $^3\Sigma_u^+$

Potential curves for these symmetries are shown in Fig. 6. These potential curves were determined in a modified cc-pVQZ basis. Rydberg character mixes into the wave function at energies near the ion. This character was removed by deleting the most diffuse contracted functions in the s and p basis, i.e., a [4s, 3p, 3d, 2f, 1g] set was used. Because the curves are plotted with the ion placed at the experimental R_e and T_e above $X^1\Sigma_g^+$ calculated in the cc-pVQZ basis, the $^3\Delta_u$ and $^3\Sigma_u^+$ curves have been lowered by 0.065939 a.u., the energy difference between the ground states calculated in the cc-pVQZ and [4s, 3p, 3d, 2f, 1g] bases. The CASSCF for the triplet states uses a five root average and the MRCI solves for five triplet roots of which the lowest three are shown in Fig. 6. At R = 1.7 – 1.8 a_o only the lowest two roots were determined in the MRCI ($^3\Delta_u$ and $^3\Sigma_u^+$). For R > 6.8 a_o, the CASSCF orbitals were obtained from $X^1\Sigma_g^+$ due to convergence difficulties. Of these states, only $2^3\Sigma_u^+$ may be a minor route for DR.

F. $^3\Delta_g$, $^1\Delta_g$, and $^3\Sigma_g^+$

The $^3\Delta_g$ CASSCF orbitals were optimized for the lowest state only in the cc-pVQZ[52] basis and three states were obtained in the MRCI. The G and 2 states cross the ion near the large R turning points of v = 0 and v = 4, respectively (see Fig. 6). The calculations were done in A_g symmetry of D_{2h} and the second state is $^3\Sigma_g^+$. The $^3\Sigma_g^+$ state crosses the large R turning point of v = 4.

The $^1\Delta_g$ states, shown in Fig. 5, were calculated in B_{1g} symmetry in the cc-pVQZ[52] basis. The lowest three routes were averaged in the CASSCF and five routes were obtained in the MRCI.

$1^1\Delta_g$, $2^1\Delta_g$, and $3^1\Delta_g$ cross the ion between the outer turning points of v = 1 and 2 and at the outer turning points of v = 3, and v = 4, respectively.

G. Π_g

The $^3\Pi_g$ CASSCF averaged the orbitals over the lowest three states in the cc-pVQZ[52] basis and the lowest three states were determined in the MRCI. The lowest state, $B^3\Pi_g$ (see Table II) is too low in energy to play a significant role in DR. The $2^3\Pi_g$ state crosses the ion at the large R turning point of v = 4 (see Fig. 6). $3^3\Pi_g$ is too high in energy to play a role in DR. For the $^1\Pi_g$ states, the same approach was used as for $^3\Pi_g$. The a state is too low in energy (see Table II) and the 2, 3 states are too high in energy to be important states in DR (see Fig. 6).

H. Potential curve summary

Of the 12 potential symmetries that may play a role in DR (see beginning of Sec. II), the potential curve calculations show that the following 15 valence states in 10 symmetries are potential candidates for DR: 2-4$^3\Pi_u$, 2,3$^1\Pi_u$, $2^1\Sigma_g^+$, $b'^1\Sigma_u^+$, $2^3\Sigma_u^+$, $2^3\Pi_g$, $G^3\Delta_g$, $2^3\Delta_g$, $^3\Sigma_g^+$, and 1-3$^1\Delta_g$.

III. ELECTRONIC WIDTHS AND QUANTUM DEFECTS

Near R_e, the $X^2\Sigma_g^+$ and $A^2\Pi_u$ states of N_2^+ have the main configurations

$$\ldots 3\sigma_g\, 1\pi_{ux}^2\, 1\pi_{uy}^2 \tag{3}$$

and

$$\ldots 3\sigma_g^2\, 1\pi_{ux}\, 1\pi_{uy}^2, \tag{4}$$

respectively. Here … denotes $1\sigma_g^2 1\sigma_u^2 2\sigma_g^2 2\sigma_u^2$. The Rydberg states of N_2 described here are built upon the X and A ion cores. The electronic width, $\Gamma^{\varepsilon}_{ion,d}(R)$, connecting an ion state coupled to a free electron of energy ε with dissociative state (d) at internuclear distance R is given by

$$\Gamma^{\varepsilon}_{ion,d}(R) = 2\pi\, \langle\{\Phi_{ion}(R)\varphi_{\varepsilon}(R)\}\,|H|\,\Phi_d(R)\rangle^2 . \tag{5}$$

Clearly, the width will vanish unless both wave functions have the same electronic symmetry. Instead of using a free electron wave function for φ_ε it is computationally easier to substitute a Rydberg orbital with principal quantum number n*, multiplied by a density of states, ρ:

$$\Gamma^{\varepsilon}_{ion,d}(R) = 2\pi\rho^{n^*} \left\langle\{\Phi_{ion}(R)\varphi^{n^*}(R)\}\,|H|\,\Phi_d(R)\right\rangle^2 , \tag{6}$$

where $n^* = n - \mu$ and μ is the quantum defect. This substitution allows for the usage of bound state techniques for the calculation of the widths. The density of states is given by

$$\rho^{n^*} = 1/(E\left(n^* - \frac{1}{2}\right) - E\left(n^* + \frac{1}{2}\right)) \approx n^{*^3} \tag{7}$$

and ρ^{n^*} has inverse energy units. The width resulting from the use of Eq. (6) corresponds to capture of a zero energy electron. (Note that the square of the matrix element on the right side of Eq. (6) varies as $1/n^{*3}$ due to the normalization of the Rydberg orbital.)

In the width calculations, the valence orbitals for both the dissociative states and the ion are expanded in a cc-pVDZ (Ref. 52) basis and the Rydberg orbitals are expanded in the same basis plus 18 diffuse Gaussians centered at the midpoint

with Gaussian exponents given by the formulas of Kaufmann *et al.*[66] The improved virtual orbital (IVO) method[67] is used for the calculation of the Rydberg orbitals. The widths are calculated using the highest n* orbital that is accurately described by the basis. In most cases, n* = 9 orbitals are used.

Three types of widths are needed for the cross section calculations. The width for electron capture by the ground ion state into a dissociative state is needed to describe direct DR and some aspects of indirect DR. This is the same matrix element that is needed to describe predissociation of ground core Rydberg states by the dissociative state. Although DR of the $A^2\Pi_u$ state is not described in these calculations, capture of an electron into an A core Rydberg state can occur via a second order electronic mechanism in which the dissociative state connects an A core Rydberg state to the X core plus a free electron (see below).[33] In order to describe this mechanism, a width similar to (6) is needed in which the ground ion core is replaced by the A core. The last type of width involves a first order capture of the incoming electron in the field of the ground state ion into an A core Rydberg state. In this width matrix element, $\Phi_{ion}(R)$ in (6) is the ground state ion but the dissociative state is replaced by the A core state plus a Rydberg or continuum electron (see Eq. (14) below). The width calculations are described below for each electronic symmetry.

A. $^3\Pi_u$

For $^3\Pi_u$ total symmetry, the Rydberg orbital in the field of $X^2\Sigma_g^+$ must be $n\pi_{ux}$ or $n\pi_{uy}$ With the main configuration of the ion ground state given in (3), the Rydberg orbitals are eigenfunctions of the IVO Hamiltonian:

$$H(X,{}^3\Pi_u) = h + \sum_i 2J_i - K_i + J_{3\sigma_g} - K_{3\sigma_g}, \qquad (8)$$

where h contains the one electron terms (kinetic energy plus nuclear repulsion) and i runs over the closed shell orbitals, i.e., all the orbitals in (3) except $3\sigma_g$. J and K are coulomb and exchange operators, respectively. The Rydberg orbitals are expanded in the valence basis set supplemented by 18 $2p\pi_x$ diffuse Gaussian primitives[66] centered at the midpoint of the internuclear axis. With the diffuse functions at the midpoint, the calculated widths are reliable only for small internuclear distances, i.e., R $<\approx$ 2.7 a_o and the widths are most accurate for high Rydberg orbitals, i.e., n = 8 or 9.

The orbitals used in the calculation of $\Phi_{ion}(R)$ and $\Phi_d(R)$ in Eq. (6) and in the construction of the coulomb and exchange operators in (8) are determined in CASSCF calculations for $X^2\Sigma_g^+$ in which the $2\sigma_g$, $2\sigma_u$, $3\sigma_g$, $3\sigma_u$, $1\pi_{ux}$, $1\pi_{gx}$, $1\pi_{uy}$, and $1\pi_{gy}$ orbitals are active. The $np\pi_{ux}$ orbitals from the IVO calculation are orthogonalized to the CASSCF π_u virtual orbitals. The $\Phi_{ion}(R)\varphi^{n^*}$ reference wave function is formed by coupling the IVO orbital and each of the CASSCF virtual π_u orbitals to each of the 10 configurations needed for the correct dissociation of the ion wave function giving total $^3\Pi_{ux}$ symmetry. The wave function is restricted to all single and double excitations within the $2\sigma_g - 3\sigma_u$, $1\pi_u$, $1\pi_g$ orbitals including the 2, $3\pi_{ux}$ virtuals and the $n\pi_{ux}$ orbital. Each configuration is restricted to have a single electron in either the 2, $3\pi_{ux}$ virtual orbitals or the Rydberg orbital. Using the same ion orbitals, the Φ_d wave function is a full CI within the $2\sigma_g - 3\sigma_u$ and the $1\pi_u$, $1\pi_g$ orbital spaces. The 1σ orbitals were kept doubly occupied in both the Rydberg and dissociative wave functions. With this approach, the Rydberg and valence CI wave functions are disjoint and orthogonal.[68] The Rydberg space is also augmented with virtual roots from the dissociative state calculation. This approach, described previously,[36,69] adds additional correlation to the Rydberg wave function. Of the 192 roots of the dissociative CI, the 182 highest energy roots were allowed to mix into the Rydberg wave function. The $^3\Pi_u$ widths are given in Table III for the ground ion core and are shifted in R to correct for the difference between experimentally and theoretically derived R_e values for the ion in these small wave functions (0.0398 a_o). No comparison is made here to the experimentally derived[56] width since the latter is R independent and for the lowest Rydberg state. The width calculated here from an n = 9 Rydberg state is 0.16 eV for $2^3\Pi_u$ at R = 2.0602 a_o (see Table III).

TABLE III. $^3\Pi_u$ electronic widths for $X^2\Sigma_g^+$ (eV).

R(a_o)[a]	$C^3\Pi_u$	$2^3\Pi_u$	$3^3\Pi_u$	$4^3\Pi_u$
1.8	0.065	0.095	0.00094	0.027
1.9	0.064	0.11	0.0015	0.031
2.0	0.061	0.13	0.0020	0.035
2.1	0.056	0.16	0.0023	0.039
2.2	0.048	0.18	0.0023	0.043
2.3	0.039	0.21	0.0018	0.048
2.4	0.031	0.25	0.0012	0.053
2.5	0.022	0.29	0.0007	0.058
2.6	0.017	0.34	0.0010	0.064
2.8	0.016	0.46		

[a]Subtract 0.0398 to get R.

For the $A^2\Pi_u$ ion core, the widths are calculated in an analogous manner except that for total $^3\Pi_{ux}$ symmetry, the Rydberg orbital is $ns\sigma_g$ and the IVO Hamiltonian now has the form

$$H(A,{}^3\Pi_u) = h + \sum_i 2J_i - K_i + J_{1\pi_{ux}} - K_{1\pi_{ux}}, \qquad (9)$$

where i runs over the closed shell orbitals, i.e., all the orbitals in (4) except $1\pi_{ux}$. The Rydberg basis now consists of a set of diffuse s Gaussians placed at the molecular midpoint. The calculated widths for the A core ion are given in Table IV. As shown in Table IV, the $2^3\Pi_u$ widths are small with a significant variation with R. The $nd\sigma_g$ and $nd\delta_g$ Rydberg orbitals are not included in these calculations.

The primary configurations of the four $^3\Pi_u$ dissociative routes at R = 2.2 a_o are

$$C^3\Pi_u \qquad \ldots 2\sigma_g^2\, 2\sigma_u\, 3\sigma_g^2\, 1\pi_{ux}^2\, 1\pi_{uy}^2\, 1\pi_{gx}, \qquad (10)$$

$$2^3\Pi_u \qquad \begin{matrix}\ldots 2\sigma_g^2\, 2\sigma_u^2\, 3\sigma_g\, 1\pi_{ux}^2\, 1\pi_{uy}\, 1\pi_{gx}\, 1\pi_{gy} \\ \ldots 2\sigma_g^2 2\sigma_u^2 3\sigma_g 1\pi_{ux} 1\pi_{uy}^2 1\pi_{gx}^2,\end{matrix} \qquad (11)$$

$$3^3\Pi_u \qquad \ldots 2\sigma_g^2\, 2\sigma_u^2\, 3\sigma_g\, 1\pi_{ux}^2\, 1\pi_{uy}\, 1\pi_{gx}\, 1\pi_{gy}, \qquad (12)$$

TABLE IV. $^3\Pi_u$ electronic widths for $A^2\Pi_u$ (eV).

R(a_o)[a]	$C^3\Pi_u$	$2^3\Pi_u$	$3^3\Pi_u$	$4^3\Pi_u$
1.8	0.052	0.0057	0.0015	0.036
1.9	0.050	0.0048	0.0018	0.031
2.0	0.047	0.0040	0.0021	0.027
2.1	0.045	0.0033	0.0025	0.022
2.2	0.043	0.0028	0.0032	0.019
2.3	0.040	0.0024	0.0042	0.016
2.4	0.037	0.0021	0.0060	0.013
2.5	0.033	0.0020	0.0097	0.010
2.6	0.025	0.0023	0.016	0.0070

[a]Subtract 0.0469 to get R.

and

$$4\,^3\Pi_u \qquad \ldots 2\sigma_g^2\, 2\sigma_u^2\, 3\sigma_g\, 1\pi_{ux}\, 1\pi_{uy}^2\, 1\pi_{gy}^2. \tag{13}$$

The 2 state has two primary configurations one of which is identical to that of $3^3\Pi_u$ but a different spin coupling. All these configurations differ by a double excitation from the X ion state plus a free electron and the excitation difference does not account for the variation of the width magnitudes. The first configuration in (11) and that in (12) differ from the main configuration of the A ion state plus a free electron by a triple excitation and these states have the smallest widths of the four routes (with the exception of the point at R = 2.5531). The width for $3^3\Pi_u$ is too small for this channel to provide a major contribution to the DR of the X or A states. The width for $2^3\Pi_u$ with $X^2\Sigma_g^+$ plus a free electron is the largest of all the $^3\Pi_u$ widths and monotonically increases with R as does $4^3\Pi_u$.

The connecting width between ground ion core and excited ion core states contains two density of states and is given by

$$\Gamma^c = 2\pi\rho^{n_X^*}\rho^{n_A^*}\left\langle\psi^{n_X^*}|H|\psi^{n_A^*}\right\rangle^2, \tag{14}$$

where $\rho^{n_X^*}$ is the density of states for the X core Rydberg state ($\psi^{n_X^*}$) and $\rho^{n_A^*}$ is the density of states for the A core Rydberg state ($\psi^{n_A^*}$) calculated from the Rydberg energies having the n_X^* and n_A^* principal quantum numbers, respectively. Note that the width in Eq. (14) is unitless. The connecting widths are given in Table V. A comparison to the experimentally derived[56] value is not useful since the latter are R independent and are for the lowest Rydberg states. The quantum defects for the $^3\Pi_u$ series with the ground core were calculated by using an RKR fit derived[41] for the $c^1\Pi_u$ Rydberg state. The difference between the derived energy (below $X^2\Sigma_g^+$) at the inner turning point of the v = 0 level of $c^1\Pi_u$ and our calculated energy is 0.007170 a.u. This value was used to lower the calculated curve for n = 3, $^3\Pi_u$ at all R relative to the calculated ion curve. The ion wave function is generated in a manner analogous to that of the Rydberg state without 2, $3\pi_u$ virtuals, and the $n\pi_u$ orbital. The quantum defects are given in Tables VI and VII for X core Rydberg states and A core Rydberg states, respectively. For the ground state ion, $R_e = 2.11a_o$. For R = 2.0602 and 2.1602, the calculated quantum defects from Table VI are 0.7554 and 0.7450 in excellent agreement with the experimentally derived value of 0.75 (Ref. 56) for $G^3\Pi_u$. For the Rydberg states with the $A^2\Pi_u$ core, quantum defects were obtained in the width calculations using an ion wave function appropriate for the Rydberg wave function. The value of 1.010 in Table VII at R = 2.0531 a_o is in agreement with that found in the pioneering work of Lefebvre-Brion and Moser[70] at R = 2.0675 a_o of 1.17 for $4s\sigma_g$, $^3\Pi_u$. Another calculation[71] at 2.1097 found a quantum defect of 1.01 also in agreement with the current result.

TABLE V. $^3\Pi_u$ continuum-continuum electronic widths (unitless).

R(a_o)	Γ ($^3\Pi_u$)
1.7567	0.0070
1.8567	0.0066
1.9567	0.0066
2.0567	0.0059
2.1567	0.0055
2.2567	0.0048
2.3567	0.0044
2.4567	0.0037
2.5567	0.0032
2.6567	0.0027
2.7567	0.0022
2.8567	0.0017
2.9567	0.0013

B. $^1\Pi_u$

Calculation of the $^1\Pi_u$ widths follows the same course as for $^3\Pi_u$ with the necessary changes for the spin coupling, e.g., the IVO exchange operators, $K_{3\sigma_g}$ and $K_{1\pi_{ux}}$ in Eqs. (8) and (9) have positive signs. The widths are smaller than for $2^3\Pi_u$ and are 0.033, 0.058, and 0.032 eV at R = 2.0602 a_o for b, 2 and $3^1\Pi_u$. As for $^3\Pi_u$, the calculated energies for $c^1\Pi_u$ were lowered by 0.007170 a.u. at all R for the determination of the quantum defects. The quantum defect at R = 2.0602 is 0.7554.

TABLE VI. Quantum defects for $^3\Pi_u$ Rydberg states with the $X^2\Sigma_g^+$ core.

R(a_o)[a]	μ(np π_u $^3\Pi_u$)
1.8	0.7899
1.9	0.7778
2.0	0.7663
2.1	0.7554
2.2	0.7450
2.3	0.7351
2.4	0.7258
2.5	0.7170
2.6	0.7088
2.7	0.7011
2.8	0.6940
2.9	0.6874
3.0	0.6814

[a]Subtract 0.0398 to get R.

TABLE VII. Quantum defects for $^3\Pi_u$ Rydberg states with the $A^2\Pi_u$ core.

R(a_o)[a]	μ ($ns\sigma_g\ ^3\Pi_u$)
1.8	1.012
1.9	1.012
2.0	1.011
2.1	1.010
2.2	1.009
2.3	1.008
2.4	1.006
2.5	1.004
2.6	1.001
2.7	0.9971
2.8	0.9931
2.9	0.9887
3.0	0.9841

[a]Subtract 0.0469 to get R.

The primary configurations of the three $^1\Pi_u$ dissociative routes at R = 2.2 a_o are

$$b^1\Pi_u \quad \ldots 2\sigma_g^2\, 2\sigma_u\, 3\sigma_g^2\, 1\pi_{ux}^2\, 1\pi_{uy}^2\, 1\pi_{gx}, \tag{15}$$

$$\begin{aligned} 2^1\Pi_u \quad & \ldots 2\sigma_g^2\, 2\sigma_u\, 3\sigma_g^2\, 1\pi_{ux}^2\, 1\pi_{uy}^2\, 1\pi_{gx} \\ & \ldots 2\sigma_g^2\, 2\sigma_u^2\, 3\sigma_g\, 1\pi_{ux}^2\, 1\pi_{uy}\, 1\pi_{gx}\, 1\pi_{gy} \\ & \ldots 2\sigma_g^2\, 2\sigma_u^2\, 3\sigma_g\, 1\pi_{ux}\, 1\pi_{uy}^2\, 1\pi_{gx}^2, \end{aligned} \tag{16}$$

and

$$3^1\Pi_u \quad \ldots 2\sigma_g^2\, 2\sigma_u^2\, 3\sigma_g\, 1\pi_{ux}\, 1\pi_{uy}^2\, 1\pi_{gy}^2. \tag{17}$$

As expected, the primary orbital occupancies are similar to those for $^3\Pi_u$ except that the b state primary configuration is more important for $2^1\Pi_u$ than that same configuration is for $2^3\Pi_u$. The $2^1\Pi_u$ widths are smaller than those for $2^3\Pi_u$ and with a three times greater statistical weight, the triplet state is more important for DR.

C. $b'^1\Sigma_u^+$

The widths for $b'^1\Sigma_u^+$ with the $X^2\Sigma_g^+$ core plus a Rydberg electron were calculated by placing 18 diffuse pσ Gaussian primitives[66] at the molecular midpoint. For the excited $A^2\Pi_u$ core, the $^1\Sigma_u^+$ symmetry was generated by attaching a free or Rydberg electron in a dπ orbital made up in part of 18 diffuse $d\pi_{xz}$ Gaussians[66] placed at the internuclear axis midpoint. The free electron widths with the ground core (Eq. (6)) change rapidly with internuclear distance ranging from 0.89 eV at R = 2.0 a_o to 0.00040 eV at R = 2.4 a_o. The dominant configurations for b′ at R = 2.0 a_o are

$$\begin{aligned} & \ldots 2\sigma_g^2\, 2\sigma_u^2\, 3\sigma_g^2\, 1\pi_{ux}^2\, 1\pi_{uy}\, 1\pi_{gy} \\ & + \ldots 2\sigma_g^2\, 2\sigma_u^2\, 3\sigma_g^2\, 1\pi_{ux}\, 1\pi_{uy}^2\, 1\pi_{gx}, \end{aligned} \tag{18}$$

which differ by a double excitation from the ground state ion plus a Rydberg electron and by a single excitation from the A core ion plus a Rydberg electron. Matrix elements (see Eq. (6)) between states differing by a single excitation can be very large. Indeed, at R = 2.0 a_o and R = 2.4 a_o, the widths are 4.58 eV and 3.39 eV, respectively. On the other hand, the calculated Rydberg-Rydberg width (Eq. (14)) is less than 0.004 eV. The small Rydberg-Rydberg width means that a direct capture of a free electron into an excited core Rydberg level cannot occur in $^1\Sigma_u^+$ symmetry. However, the large A core width means that A core Rydberg states can be populated by a second order mechanism in which the dissociative state acts to connect the ground core and excited core states.

D. $2^1\Sigma_g^+$

The major configuration for $2^1\Sigma_g^+$ near the ion is

$$\ldots 2\sigma_g^2\, 2\sigma_u^2\, 3\sigma_g^2\, 1\pi_{ux}\, 1\pi_{uy}\, 1\pi_{gx}\, 1\pi_{gy} \tag{19}$$

and differs from the ground state ion plus a free electron by a triple excitation and a small width is expected. $X^2\Sigma_g^+$ can attach an sσ or dσ Rydberg orbital to form a $^1\Sigma_g^+$ state. Adding a diffuse basis of 18 s Gaussians[66] at the molecular midpoint gives a width that varies from 0.014 to 0.023 eV between 2.0 and 2.4 a_o. Expanding the Rydberg orbital in 18 dσ diffuse primitives,[66] the calculated width for this state is 0.011 eV to 0.014 eV between 2.0 and 2.4 a_o and has been reported previously.[24]

A double excitation from (4) plus a "free" electron is needed to generate (19). For this width, 18 diffuse pπ Gaussians[66] were placed at the molecular midpoint to give $^1\Sigma_g^+$ symmetry. These widths range from 0.15 to 0.23 eV for R between 2.0 and 2.4 a_o.

For the direct connecting width (see Eq. (14)), only the dσ wave was used for the ground core. These widths were reported previously[24] (Table VI) and were incorrect and should be divided by 27.21 to get the correct widths. The correct widths were used in the previously reported[24] calculations. The widths range from 0.0151 to 0.0143 for R = 2.0 and R = 2.4 a_o, respectively. These widths were calculated by using the n = 9 ground core Rydberg state and the n = 4 excited core state.

E. $^3\Sigma_u^+$

The $^3\Sigma_u^+$ widths were calculated in the field of the ground state ion by placing 18 diffuse pσ primitives[66] at the midpoint of the internuclear axis and following the procedure outlined above. $A^3\Sigma_u^+$ is too low in energy to contribute to DR. The most important configurations of $2^3\Sigma_u^+$ at R = 2.3 a_o are

$$\begin{aligned} & \ldots 2\sigma_g^2\, 2\sigma_u\, 3\sigma_g\, 1\pi_{ux}^2\, 1\pi_{uy}^2\, 1\pi_{gx}^2 \text{ and} \\ & \ldots 2\sigma_g^2\, 2\sigma_u\, 3\sigma_g\, 1\pi_{ux}^2\, 1\pi_{uy}^2\, 1\pi_{gy}^2. \end{aligned} \tag{20}$$

These differ by a double excitation from the ion ground state plus a free electron indicating that the width may be non-negligible. $2^3\Sigma_u^+$, which crosses the large R turning point of v = 4, has an electron capture width of 0.16–0.61 eV in the region between 2.2 and 2.4 a_o. Excited core states were not included for this symmetry.

F. G-$2^3\Delta_g$, 1-$3^1\Delta_g$

Using an approach similar to that described above, 18 $d\delta_{xy}$ Gaussian primitives[66] have been placed at the molecu-

lar midpoint. At $\mathbf{R} = 2.0$ a_o, the main configurations of the $G^3\Delta_g$ state in $^3B_{1g}$ symmetry of D_{2h} are the degenerate terms

$$\ldots 2\sigma_g^2\, 2\sigma_u^2\, 3\sigma_g^2\, 1\pi_{uy}^2\, 1\pi_{gx}\, 1\pi_{gy} + \ldots 2\sigma_g^2\, 2\sigma_u^2\, 3\sigma_g^2\, 1\pi_{ux}^2\, 1\pi_{gx}\, 1\pi_{gy}. \quad (21)$$

These configurations differ from the main configuration of the ground state ion plus a free electron by a triple excitation and the width matrix element contribution vanishes for the most important configurations. The calculated electronic width for this state at R = 2.1 a_o is 1×10^{-5} eV. That for $2^3\Delta_g$ is 0.0011 eV.

For $1^1\Delta_g$, the most important configuration near the ion crossing is

$$\ldots 2\sigma_g^2\, 2\sigma_u^2\, 1\pi_{ux}^2 1\pi_{uy}^2\, 1\pi_{gx}\, 1\pi_{gy}. \quad (22)$$

This configuration differs by a double excitation from the main configuration of the ground state ion plus a free electron. The calculated width ranges from 0.011 eV at 2.0 a_o to 0.0058 eV at 2.4 a_o. The main configurations of $2^1\Delta_g$ are mostly

$$\ldots 2\sigma_g^2\, 2\sigma_u^2\, 3\sigma_g^2\, 1\pi_{ux}\, 1\pi_{uy}\, 1\pi_{gx}^2 + \ldots 2\sigma_g^2\, 2\sigma_u^2\, 3\sigma_g^2\, 1\pi_{ux}\, 1\pi_{uy}\, 1\pi_{gy}^2 \quad (23)$$

followed by (21) and (22). $3^1\Delta_g$ consists mostly of (21) and (23). Since (21) and (23) differ by a triple excitation from the main configuration of the ground ion plus a free electron the 2 and $3^1\Delta_g$ widths are small, i.e., less than 5×10^{-4} eV. Excited core states were not included for this symmetry.

G. $^3\Sigma_g^+$

For the $^3\Sigma_g^+$ widths, basis sets of sσ and dσ functions each having 18 diffuse primitives[66] are placed at the molecular midpoint. The main configuration of the dissociative state at R = 2.4 a_o is

$$\ldots 2\sigma_g^2\, 2\sigma_u^2\, 3\sigma_g^2 1\pi_{ux} 1\pi_{uy}\, 1\pi_{gx}\, 1\pi_{gy}, \quad (24)$$

the same as $G^3\Delta_g$. A triple excitation must be applied to (24) to obtain the ground state ion plus a free electron and the widths are small. The potential curve crosses the outer turning point of v = 4 and the width at R = 2.4 a_o is 0.01 eV for sσ and 0.00005 eV for dσ both calculated with n = 9 Rydberg orbitals.

H. $^3\Pi_g$

$B^3\Pi_g$ (see Table II) and $3^3\Pi_g$ (see Fig. 6) are too low and high, respectively, to contribute to DR but $2^3\Pi_g$ could be important for v = 4. The main configuration of $2^3\Pi_g$ near the ion crossing in the cc-pVQZ potential curve calculation is

$$\ldots 2\sigma_g^2\, 2\sigma_u^2\, 3\sigma_g^2\, 3\sigma_u\, 1\pi_{ux}\, 1\pi_{uy}^2, \quad (25)$$

which differs by a double excitation from the ion ground state plus a free electron. Eighteen diffuse dπ Gaussians[66] were placed at the molecular midpoint for the width calculation. Instead of using orbitals for $X^2\Sigma_g^+$ (which does not give sufficient weight to the $3\sigma_u$ orbital) orbitals optimized for $2^3\Pi_g$ were used in the width calculations. Between R = 2.1 and 2.4 a_o the calculated width, determined from the n = 10 Rydberg orbital, is less than 0.003 eV.

I. Electronic width and potential curve summary

From the calculated potential curves and widths, the 14 following states may be important for DR and are included in the cross section and rate constant calculations described below: C-$4^3\Pi_u$, b, 2, $3^1\Pi_u$, $2^1\Sigma_g^+$, $b'^1\Sigma_u^+$, $2^3\Sigma_u^+$, $2^3\Pi_g$, $^3\Sigma_g^+$, $1^1\Delta_g$, and $2^3\Delta_g$.

IV. CROSS SECTIONS

A. Approach

The MQDT approach, used for the calculation of the cross sections, has been described in detail elsewhere[33,72] and only a summary is provided here.

As in the earlier work,[33,72] the short range interactions between the dissociative and ion or Rydberg states are included in a K matrix which is based upon the Lippmann-Schwinger equation. The K matrix contains all the couplings between channels where a channel is defined as either a dissociative vibrational state or a bound ion vibrational state. With the electron-ion and dissociative states coupled by the electronic width matrix elements, the couplings are given by

$$V_{id}(\mathrm{R}) = \langle \chi_i(\mathrm{R}) | (\Gamma_{ion,d}(R)/2\pi)^{1/2} | \chi_d(R) \rangle \quad (26)$$

and

$$V_{ii'}(\mathrm{R}) = \langle \chi_i(\mathrm{R}) | (\Gamma^c(R)/2\pi)^{1/2} | \chi_{i'}(R) \rangle \quad (27)$$

(see Eqs. (5), (6), and (14)). Here χ_i and χ_d are vibrational wave functions for the ion and dissociative states and the integration is over R. The K matrix is given by

$$K = V + VGK, \quad (28)$$

where G is the standing wave Green operator. In first order, $K = V$ and the matrix elements in Eqs. (26) and (27) are the sole components of the K matrix. Note that this definition differs slightly from the prior definition[33,72] because we include at first order the excited core states through $V_{ii'}$. Because K appears on both sides of Eq. (28), this is a perturbative approach which is calculated here to second order, i.e., $K = V + VGV$. The reduction of VGV to a workable form has been described.[33] $K_{ii'}$ contains both the first order component $V_{ii'}$ and a second order component in which the dissociative state connects two electron-ion states. If the set of vibrational levels in the $X^2\Sigma_g^+$ and $A^2\Pi_u$ states are denoted $\tilde{X}$ and $\tilde{A}$, respectively then $V_{ii'} = 0$ if $i, i' \in \tilde{X}$ or $i, i' \in \tilde{A}$ because the connecting width, $\Gamma^c = 0$. The first order component is nonzero only if $i \in \tilde{X}$ and $i' \in \tilde{A}$ or vice versa. For the second order component, these restrictions do not apply and all electron ion channels are connected through the dissociative state. The second order component can be written as

(see Eq. (34) of Ref. 33):

$$K_{ii'} = \left(\frac{1}{\omega}\right)\int\int \chi_i(R)(\Gamma_{ion,d}(R)/2\pi)^{\frac{1}{2}} F_d(R_<)G_d(R_>) \times (\Gamma_{ion,d}(R')/2\pi)^{1/2}\chi_{i'}(R')dRdR', \quad (29)$$

where F_d and G_d are regular and irregular dissociative wave functions, $R_<$ and $R_>$ are the lesser and greater of R and R', respectively and ω is the Wronskian. All these interactions are included in the MQDT approach used here.

The reaction matrix, defined as $-\pi K$, has eigenvalues $\tan\eta_\alpha$ such that

$$\sum_j -\pi K_{ij}U_{j\alpha} = -\tan\eta_\alpha U_{i\alpha}. \quad (30)$$

It has been shown[72] that near the molecule, the full eigenchannel wave function can be written as a superposition of dissociative and ion plus electron wave functions where the superposition coefficients are given by the eigenvectors of the K matrix, $U_{j\alpha}$. The nuclear dissociative and electronic ion plus electron wave functions each consist of a regular and irregular part with coefficients $\cos\eta_\alpha$ and $\sin\eta_\alpha$, respectively. A frame transformation is then used in which the wave function far from the molecule is written as a superposition of R independent terms with R independent coefficients, C and S. Equating the two wave functions at the boundary between the inner and outer regions allows for the determination of C and S. With these coefficients, the matrix X is calculated, $X = (C+iS)/(C-iS)$, from which the scattering matrix is given by[73]

$$S_{oo} = X_{oo} - X_{oc}(X_{cc} - e^{i\pi\nu})^{-1}X_{co}, \quad (31)$$

where o and c designate open and closed channels, respectively. ν is a diagonal matrix of dimension $c \times c$ with elements $\nu_v = (2(E_v - E_T))^{-\frac{1}{2}}$. Here E_v is the energy of the closed vibrational ionization channels where E_T is the total energy. Finally, the DR cross section for ion vibrational level v is given by

$$\sigma_v(\varepsilon) = \frac{\pi}{2k^2}\sum_d\sum_{\ell_d} r_d\left|S(\varepsilon)^{\ell_d}_{d,v}\right|^2, \quad (32)$$

where v is the ion vibrational level, ε is the electron energy, r_d is the ratio of multiplicities of the final neutral state to the ion state, k is the electron wave number, $k = (2m\varepsilon)^{1/2}$, m is the electron mass, d is the dissociative state, and ℓ_d is an index for the angular momentum quantum number of the "free" electron being captured into dissociative state, d. In the calculations reported below, d runs over the 14 dissociative states discussed in the prior sections.

All vibrational wave functions were calculated on a grid of 0.001 a_o between 1.0 and 8.0 a_o. Cross sections were calculated between 0.0001 and 1.0 eV on a 0.0001 eV grid up to 0.1 eV where the grid is changed to 0.001 eV. The lowest 18 vibrational levels in $X^2\Sigma_g^+$ and in $A^2\Pi_u$ are included in the calculations. Each Rydberg state also includes 18 vibrational levels.

As mentioned above, 14 dissociative states are included. For both $2^1\Sigma_g^+$ and $^3\Sigma_g^+$ two partial waves for the incoming electron are treated giving a total of 16 capture channels for the $X^2\Sigma_g^+$ ground state. For each of the 16 channels, a Rydberg series of the same electronic symmetry is included. Between 0.0 and 1.0 eV electron energy, the v = 1, 2, and 3 ion vibrational levels are Rydberg series limits for each capture channel. Therefore, a total of 48 series of Rydberg levels are included in the calculations. Also included are the capture channels for $A^2\Pi_u$. The excited ion core is accounted for in four symmetries: $^3\Pi_u$, $^1\Pi_u$, $^1\Sigma_g^+$, and $^1\Sigma_u^+$ adding five capture channels ($2^1\Sigma_g^+$ has two partial waves). Because the electron energy is limited to less than 1.0 eV in this study and v = 0 $A^2\Pi_u$ lies at 1.12 eV above the v = 0 ion ground state, no infinite Rydberg series leading to the excited core falls within this range. However, the full Rydberg series, up to 1 eV, for each of the five excited core capture channels is included.

B. Results

1. 0.001–0.1 eV electron energy

The spectroscopic identification of states below the ion is a challenging exercise because of the many close lying states and the interference between them. Above the ion, autoionization adds to the challenge. However, the interactions included in prior spectroscopic studies at energies below the ion are included in the MQDT approach that is used here (in addition to autoionization). For $^3\Pi_u$, these interactions include those between the $np\pi_u$ Rydberg series having the ground ion as core and the $ns\sigma_g$ series having the A state as core in addition to the interactions between each series member and the four $^3\Pi_u$ dissociative valence states. Because the Rydberg states are the source of most of the cross section structure, the DR cross section is an above threshold spectrum in which it is possible to identify resonant states just as one would in a photoionization spectrum.

The total DR cross section for v = 0 is shown in Fig. 7 for electron energies up to 0.1 eV along with the total and individual cross sections for all four $^3\Pi_u$ states. $2^3\Pi_u$ is the main component of the cross section at most energies. A separate calculation of the positions of the resonance states using only

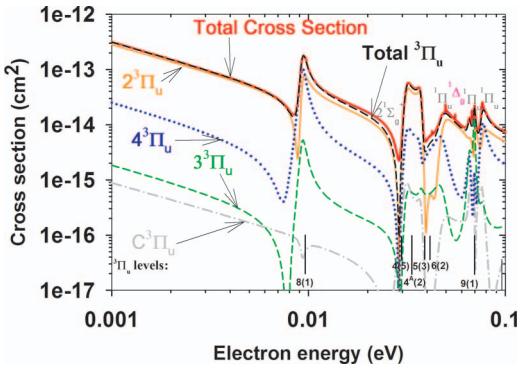

FIG. 7. Total DR cross section (thick red line) for v = 0 having contributions from 16 dissociative states is shown with the total $^3\Pi_u$ cross section (long black dashes) and that for $C^3\Pi_u$ (gray dot-dashed line), $2^3\Pi_u$ (thin solid orange line), $3^3\Pi_u$ (short green dashes) and $4^3\Pi_u$ (blue dotted line). The small state symbols without arrows indicate the sources of cross section features. The positions of $^3\Pi_u$ resonances are shown at the bottom. $4^A(2)$ is an excited core n = 4, v = 2 resonance.

TABLE VIII. Calculated $X^2\Sigma_g^+(np\pi_u)$ and $A^2\Pi_u$ $(ns\sigma_g)$ $^3\Pi_u$ Rydberg vibrational levels at 0.0 – 1.0 eV electron energy above v = 0 ion level (from the Rydberg formula only).[a,b]

Energy (above v = 0) eV	n	v	Energy (above v = 0) eV	n	v
0.0092	8	1	0.57[A]	6	0
0.024	4	5	0.60	9	3
0.042	6	2	0.63[A]	F	14
0.045	5	3	0.64	10	3
0.061[A]	F	11	0.67	11	3
0.061[A]	4	2	0.69	12	3
0.068	9	1	0.71	13	3
0.089	G	11	0.71	7	4
0.11	10	1	0.72[A]	4	5
0.14	11	1	0.73[A]	5	2
0.16	12	1	0.74[A]	7	0
0.18	13	1	0.76	G	14
0.19	7	2	0.80	8	4
0.25[A]	F	12	0.80	5	6
0.27[A]	5	0	0.81[A]	6	1
0.28	8	2	0.81	6	5
0.29[A]	4	3	0.82[A]	F	15
0.30	5	4	0.84[A]	8	0
0.30	6	3	0.85	9	4
0.32	G	12	0.89	10	4
0.34	9	2	0.91[A]	9	0
0.38	10	2	0.92	11	4
0.41	11	2	0.94[A]	4	6
0.43	12	2	0.95	12	4
0.44	13	2	0.95[A]	5	3
0.44[A]	F	13	0.95[A]	10	0
0.45	7	3	0.96	13	4
0.50[A]	5	1	0.96	7	5
0.51[A]	4	4	0.97	G	15
0.52	4	7	0.97[A]	7	1
0.54	G	13	0.98[A]	11	0
0.54	8	3	0.99	4	9
0.56	5	5	1.0[A]	F	16
0.56	6	4			

[a]G and F denote the n = 3 levels with the ground core and excited core, respectively.
[b]The superscript A in the Energy column denotes states having the $A^2\Pi_u$ core.

0.27 4 6 0.76 4 8

the variation of the quantum defect with R, i.e., without allowing for any of the interactions mentioned in the preceding paragraph, predicts that there are 69 resonances, i.e., 69 $^3\Pi_u$ Rydberg vibrational states with either an $ns\sigma_g$ or $np\pi_u$ outer orbital in the region between 0 and 1.0 eV (see Table VIII) above the $X^2\Sigma_g^+$ v = 0 level if each infinite series of resonances is cut off at n = 13. (The $nd\sigma_g$ and $nd\delta_g$ states with the A core are not treated in this study.) n > 13 states are included in the MQDT calculation and n is limited only by the interval used in the energy grid. The eight resonances between 0 and 0.1 eV above v = 0 are (n(v)): 8(1) at 0.0092 eV, 4(5) at 0.024, 6(2) at 0.042, 5(3) at 0.045, F(11) at 0.061, 4(2)[A] at 0.061, 9(1) at 0.068 and G(11) at 0.089 eV where the A superscript indicates that this level has the A ion core. Here, the n = 3 value is replaced with the F (excited core) and G (ground core) labels. This information is very useful for identifying the source of the cross section structure although shifts due to interference can be large.

69

At the predicted position, the n = 8, v = 1 level dominates the cross section. Because of the nature of the Rydberg formula, the quantum defect becomes less important in determining the position as n increases. In addition, as n increases, the interactions of a resonance with the dissociation continua and with other resonances decreases in accord with Eqs. (6) and (14) because of the $\frac{1}{n*^{3/2}}$ factor in the normalization of the Rydberg orbitals. For n = 8, v = 1, the position of the level should be accurate to better than 0.001 eV.

The shape of a resonance in the DR cross section is determined by interference between "background" DR (direct recombination) and resonant (indirect) DR. Capture into the Rydberg state occurs by two mechanisms. The first is independent of the dissociative states and is through Born-Oppenheimer breakdown, embodied in the variation of the quantum defect with R. The second is through the electronic second order mechanism (described above) in which the dissociative states act as intermediates between a Rydberg vibrational level and the electron-ion continuum or between two Rydberg vibrational levels. The magnitude of this mechanism differs for each dissociative state because of both differing electronic widths and differing Franck-Condon factors. Previously,[33] we have shown that the shape of an isolated resonance can be given by the Fano[74] formula for the cross section near a resonance lying in a single continuum. The analogous continuum in DR is direct recombination. However, because there are four $^3\Pi_u$ dissociation continua, the Fano formula, which is appropriate for a single background continuum, cannot be used. Instead, the identity of the resonances can be deduced from the calculated positions described above and by comparing calculations that omit and contain specific resonances.

The $^3\Pi_u$ 8(1) resonance produces only a small dip in the cross section along the C state because at the energy of this level, the electron ion wave function is dominated by the resonance but the C state is too far from the resonance level to be an efficient route for dissociation. Pure dips are characteristic of situations in which indirect recombination is weak. The remaining states interacting with this resonance show destructive interference on the low energy side and constructive interference on the high energy side of the resonance center. At 0.030 eV, the resonance structure is due to a shifted 4(5) level which has shifted up in energy by roughly 6 meV. This low n resonance is broad and the identification of its resonance center can only be approximate. This resonance interferes with shifted 6(2) and 5(3) near 0.040 eV to produce a similar structure in the cross sections along all four dissociative routes including the $2^3\Pi_u$ state which dominates the cross section in this region. Also present is the broad 4(2)[A] resonance with the excited ion core. This resonance interferes with the others over a wide energy range around 0.03 eV. Its identity is determined by a comparison of calculations including all 18 ground ion levels but only v = 0–1 and v = 0–2 excited core vibrational levels. Note that between 0.031 and 0.038 eV, the C state now has a double peak indicating that indirect DR can occur through v = 5, 3, and 2 Rydberg levels along this state although the cross section remains small. The excited core levels are generally about 0.1 a_o to larger R than

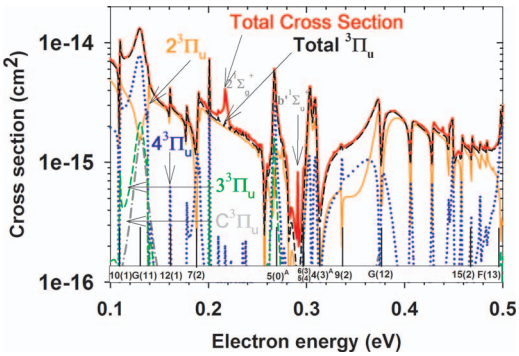

FIG. 8. Same as Fig. 7 except for 0.1–0.5 eV electron energies. G(11) is a ground core n = 3, v = 11 resonance. F(13) is an excited core n = 3, v = 11 resonance.

the ground core levels and have little interaction with the C state.

At 0.029 eV, dissociation along $2^1\Sigma_g^+$ occurs and interferes with a precipitous drop in the cross section due to the broad F(11) state. Interference between 5(3), 6(2), F(11), and $4(2)^A$ produces a peak in the $2^3\Pi_u$ cross section which dominates the structure near 0.050 eV. At and above this energy, DR along $1^1\Delta_g$ and $2^1\Pi_u$ produces narrow spikes in the DR cross section. This is unexpected considering that both states cross the ion between v = 1 and v = 2 and demonstrates further the important role of small contributions to the cross section. In the region between 0.065 and 0.080 eV the structure is due to interference among F(11), $4(2)^A$, and 9(1). Of additional interest is that at 0.0085–0.0094 eV, 0.039–0.047 eV, and 0.074–0.078 eV the $4^3\Pi_u$ state, which crosses the ion at the outer turning point of v = 1, has a larger contribution to the total cross section than $2^3\Pi_u$ and this is entirely due to resonances.

Although G(11) is expected to be mostly near 0.089 eV according to Table VIII, it is shifted up in energy and appears instead in Figure 8.

2. 0.1–0.5 eV electron energy

Figure 8 shows a remarkable cross section structure near 0.13 eV where the $C^3\Pi_u$ state, a state that does not cross the ion, has nearly the same cross section as $2^3\Pi_u$, the most important DR state for N_2^+ at most electron energies. The source of this effect is G(11) which has a peak in the C cross section but a dip in the $2^3\Pi_u$ cross section. This clearly shows that the C state, which might be considered as a negligible contributor to DR from its position relative to the ion (see Fig. 2), must be included if an accurate DR cross section is desired. The C state contributes about 13% of the total cross section at this energy. Near 0.13 eV, $4^3\Pi_u$ has the largest cross section contribution, again due to G(11).

An infinite number of v = 1 resonances lead to the v = 1 ion threshold at 0.268 eV. In Table VIII, the v = 1 resonances are listed only up to n = 13 at 0.18 eV although higher n resonances are apparent in Fig. 8 at 0.19 and 0.20 eV. The 10(1) to 13(1) resonances (see Table VIII) are clearly seen as sharp features in Fig. 8 in the total cross section except for 11(1) which is most clearly seen in the $2^3\Pi_u$ cross section at 0.14 eV. Higher v = 1 resonances are clearly seen above 0.2 eV in the $4^3\Pi_u$ cross section until they become too narrow to appear in the graph above 0.25 eV. Note that the 0.268 eV limit for v = 1 seems to be displaced from the little v = 1 wiggles in the graph by about 0.009 eV and this could be due to the limited range of quantum defects (only out to 3.0 a_o) that we have used.

The peak in the total cross section at 0.22 eV is due to dissociation along $2^1\Sigma_g^+$ and capture of a dσ partial wave by the ground core, another example of a peak due to a minor route. The peaks near 0.2 and 0.26 eV are due to $4^3\Pi_u$.

The peak at 0.27 and the double peak near 0.30 eV are in the region of several of the resonances listed in Table VIII. Of particular importance is the first v = 0 excited core resonance. A calculation without excited core states compared to one having only the v = 0 excited core level clearly identifies $5(0)^A$ as the source of the 0.27 eV peak. This level has previously been reported at 0.19 eV (Ref. 75) and the difference in positions may be due to the omission of A core Rydberg states with 3dσ and 3dδ partial waves in the current work. The higher of the two peaks at 0.30 eV also vanishes without the excited core levels but the inner peak remains. The inner peak is due to 6(3) and 5(4). $4(3)^A$ is the source of the outer peak. $b'^1\Sigma_u^+$ is the source of the sharp spike seen at 0.29 eV. A series of v = 2 resonances can be seen starting with n = 9 at 0.34 eV and falling at the energies given in Table VIII (where the series is arbitrarily terminated at 13(2)). These peaks fall on an envelope due to G(12) which runs from approximately 0.31 to 0.49 eV. Sharp peaks going up to 17(2) are shown in the figure and can be easily seen in the $4^3\Pi_u$ cross section. Near 0.45 eV, 7(3) interferes with the v = 2 series. Above 0.47 eV, a shifted F(13) becomes evident and interferes with the v = 2 series which terminates at 0.535 eV. Note that F(13) boosts the amplitude of the $4^3\Pi_u$ contribution and decreases that of $2^3\Pi_u$ as G(11) did at 0.13 eV.

At 0.32–0.46 eV, $4^3\Pi_u$ contributes more to the cross section than $2^3\Pi_u$.

3. 0.5–1.0 eV electron energy

The many oscillations in the cross section between 0.500 and 0.535 are due in part to the v = 2 series which terminates at the v = 2 ion level at 0.535 eV.

A calculation without excited core levels shows that the high peak in Fig. 9 at 0.5 eV is due to F(13) as described in the prior section. At 0.53 eV, the double peak arises from interference between $5(1)^A$ and $4(4)^A$. The large dip at 0.54 eV is due to 4(7). The peak in the 0.54–0.56 region is due mostly to G(13). At 0.57 eV, $6(0)^A$ is dominant and interferes with the first member of the above threshold v = 4 series, n = 6. 9(3) at 0.60 eV can be clearly seen as can the higher v = 3 levels given in Table VIII. These continue up to the limit at 0.797 eV.

The three peaks at 0.65, 0.66, and 0.68 eV are excited core $^1\Sigma_g^+$ levels. The second peak of the v = 4 series, n = 7, can be seen at 0.71 eV. The high peaks at 0.73, 0.74, and 0.84, 0.91, 0.93, 0.95, 0.97, and the sharp increase at 0.99 eV are all due to excited core levels. The big dip at 0.96 eV is 7(5)

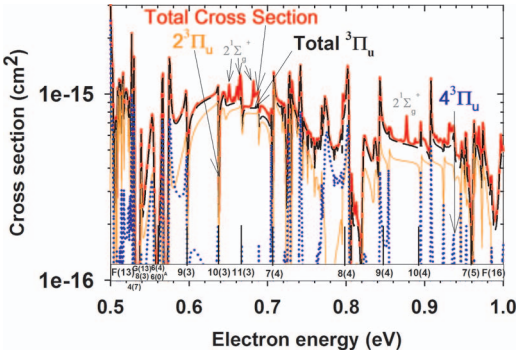

FIG. 9. Same as Fig. 8 but for electron energies from 0.5–to 0.1 eV.

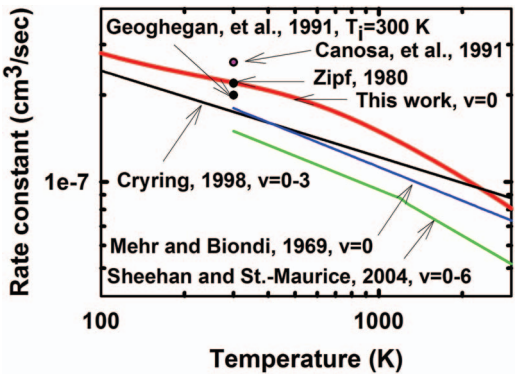

FIG. 10. Total N_2^+ DR rate constants from this work and from storage ring and afterglow experiments.

and the peak at 1.0 eV is due to F(16). The v = 4 limit is at 1.05 eV, just beyond the range of Fig. 9.

Over almost the full range in Fig. 9, the dominant dissociative route is $2^3\Pi_u$ although from 0.77—to 0.80 eV, $4^3\Pi_u$ has a larger cross section.

The first storage ring study[16] of N_2^+ DR was for $^{14}N^{15}N^+$ and only for zero electron energy. In the second study,[17] the N_2^+ was vibrationally excited. A comparison to the latter results will appear in a follow on paper of the DR of vibrationally excited N_2^+.[76]

V. RATE CONSTANTS

The rate coefficient is calculated by a Maxwellian average of the cross section over the electron energy. In contrast to the cross sections where eight dissociative states and the associated Rydberg series contribute to v = 0 DR between 0 and 1 eV, a smaller set of dissociative states suffices to describe the rate constant between $100 \le T_e \le 3000$ K. At 300 K, the direct DR rate constant due to only $2^3\Pi_u$is 2.6×10^{-7} cm^3/s. Adding the Rydberg states reduces the rate constant to 1.3×10^{-7} cm^3/s. With the addition of the other three $^3\Pi_u$ states, the rate constant increases to 1.8×10^{-7} cm^3/s with a 24% contribution from $4^3\Pi_u$. Including the excited core Rydberg states increases the rate constant further to 2.0×10^{-7} cm^3/s. A further 5% to 7% increase is due to $2^1\Sigma_g^+$.

From an estimated uncertainty in the intersection point of the $^3\Pi_u$ curves with the ion of ± 0.006 a_o and an estimated uncertainty in the widths of $\pm 15\%$, the total calculated rate coefficient at 300 K is $2.2^{+0.2}_{-0.4} \times 10^{-7}$ cm^3/s. A least squares fit of the rate constant for electron temperatures, $100 \le T_e \le 3000$ K gives α (100–3000) $= 2.1 \times (T_e/300)^{-0.40} \times 10^{-7}$ cm^3/s. An improved representation is obtained with fits over narrower electron temperature ranges: α (100–600) $= 2.2 \times (T_e/300)^{-0.22} \times 10^{-7}$ cm^3/s and α (601–3000) $= 1.1 \times (T_e/1800)^{-0.51} \times 10^{-7}$ cm^3/s.

The only prior theoretical study[77] from another laboratory was only partially *ab initio*. Empirical adjustments were incorporated into the potential curves and all rate constants were normalized to the experimental value at 300 K. In agreement with the current work, $2^3\Pi_u$ was found to be the most important dissociative channel. The second most important channel was found to be $3^3\Pi_u$ rather than $4^3\Pi_u$ as reported here.

A comparison of prior experimental determinations of the rate constant to the present results is given in Fig. 10. The early afterglow measurements of N_2^+ DR obtained high values, e.g., 1.2×10^{-6} cm^3/s (Ref. 7) at 300 K and 4.0×10^{-7} cm^3/s (Ref. 7) at 400 K because mass spectrometers were not used to identify the recombining species. These included both N_2^+ and N_4^+. One of the earliest microwave afterglow mass spectrometer studies[5] over the range $300 \le T_e \le 5000$ K found $\alpha = 1.8\ ^{+0.4}_{-0.2} \times (T_e/300)^{-0.39} \times 10^{-7}$ cm^3/s (see Fig. 10) in excellent agreement with the present results. An early flowing afterglow experiment[78] found a value of $2.2 \pm 0.4 \times 10^{-7}$ cm^3/s at 300 K and a shock tube measurement[13] claimed to be for v = 0, found a value of $1.78 \times (T_e/300)^{-0.37} \times 10^{-7}$ cm^3/s, both in agreement with the current result.

The first reported[79] merged beams rate constant was 1.8×10^{-7} cm^3/s at 300 K (after correcting for the factor of two calibration error) (Ref. 80). From a plasma spectroscopy experiment, Zipf[9] reported a value of $\alpha = 2.15 \times 10^{-7}$ cm^3/s for v = 0 and a flowing afterglow Langmuir probe experiment[12] (FALP) gave a rate coefficient at 300 K of 2×10^{-7} cm^3/s, all (see Fig. 10) in agreement with the current results. A merged beams experiment[15] reported a cross section that was a factor of five smaller than prior results and was later described as possibly having a calibration error.[81] An analysis[82] of the merged beams result, came to the conclusion that it could not be correct. A later merged beams experiment[83] having vibrationally excited ions found a rate coefficient of $1.5 \pm 0.23 \times (T_e/300)^{-0.39} \times 10^{-7}$ cm^3/s (see Fig. 10). The same report referred to the earlier merged beams result as a mystery that was attributed to ion vibrational excitation and discounted the possibility of calibration error. Further comment on this rate coefficient is delayed until the follow-on paper on vibrationally excited rate coefficients.[76]

An analysis of Zipf's rate constant,[82] taking into account prior objections,[84] came to the conclusion that the rate constant needed to be revised to 2.6×10^{-7} cm^3/s at 300 K. The proposed revision was in agreement with a FALP experiment[11] that found a rate coefficient of 2.6 (± 0.4) $\times 10^{-7}$ cm^3/s for v = 0 at 300 K in agreement with the current theoretically determined value.

The sole storage ring experiment[17] to measure a rate coefficient found a value of $1.75 \pm 0.09 \times (T_e/300)^{-0.30} \times 10^{-7}$ cm^3/s (see Fig. 10) also in agreement with the present result

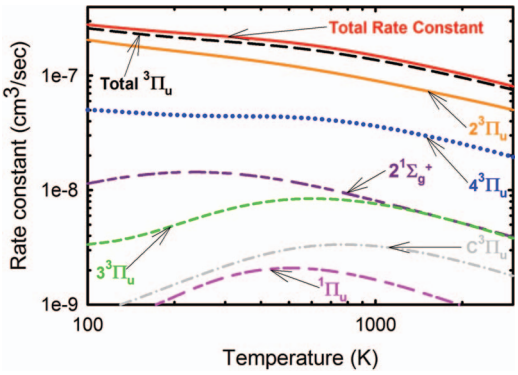

FIG. 11. The calculated total DR rate constant with the contributions from individual dissociative routes.

but for ions with substantial vibrational excitation. This will be discussed further in a separate paper on excited ion vibrational levels.[76]

Figure 11 shows the main contributions to the total rate constant for $100 \leq T_e \leq 3000$ K. The most important route at all T_e's is $2^3\Pi_u$, followed by $4^3\Pi_u$, a route that does not cross the ion within the turning points of $v = 0$. This is followed at the lower T_e's by $2^1\Sigma_g^+$ which crosses between the $v = 0$ turning points. Next in importance is $3^3\Pi_u$ which has a very small electronic width followed by $C^3\Pi_u$ which does not cross the ion curve. A recent review of the experimental studies of N_2^+ DR can be found in Ref. 85.

VI. CONCLUSIONS

The agreement between theory and experiment for the $v = 0$ rate coefficient is excellent over a wide range of electron temperatures. The DR of the $v = 0$ level of N_2^+ is dominated by $^3\Pi_u$ states, especially $2^3\Pi_u$. Many of the states considered, including the minor routes, play an insignificant role in the rate coefficient below 3000 K electron temperature. These minor routes for $v = 0$ are expected to play more important roles in the DR of excited ion vibrational levels which will be discussed separately.[76] However, in narrow energy regions, the minor routes, e.g., $C^3\Pi_u$, $3^3\Pi_u$, $4^3\Pi_u$, $b'^1\Sigma_u^+$, $1^1\Delta_g$, $2^1\Pi_u$, and $2^1\Sigma_g^+$ make nonnegligible contributions to the $v = 0$ cross section. Potential curves for the minor routes do not cross the ion between the $v = 0$ turning points with the exception of b' and $2^1\Sigma_g^+$ and one route that does not cross the ion curve. This observation has important implications for the comparison of theoretical and experimental cross sections for other ions, such as H_2^+ and H_3^+ where satisfactory agreement has not yet been achieved. Clearly, close agreement cannot be obtained between theory and future high resolution cross section measurements unless the theory includes more than just the most important channel.

Because the importance of different dissociative routes varies rapidly with electron energy there will be an equally rapid variation of the product yields. It would be very interesting for a high resolution storage ring experiment to explore this rapid variation. For example, as the electron energy increases and enters the intervals 0.0085–0.0094 eV, 0.039–0.047 eV, 0.074–0.078 eV, 0.32–0.46 eV, 0.77–0.80 eV and at 0.13 eV the theory presented here predicts that there should be a sudden doubling in the number of $N(^2D)$ atoms because of the prominence of $4^3\Pi_u$ which leads to $N(^2D) + N(^2D)$ relative to $2^3\Pi_u$ which leads to $N(^4S) + N(^2D)$.

ACKNOWLEDGMENTS

This research is supported by the National Science Foundation under Grant No. ATM-0838061 and by NASA under Grant No. NNX09AQ73G.

[1] D. R. Bates and H. S. W. Massey, Proc. R. Soc. London, Ser. A **187**, 261 (1946).
[2] J. Kaplan, Phys. Rev. **73**, 494 (1948).
[3] S. K. Mitra, Phys. Rev. **90**, 516 (1953).
[4] M. A. Biondi and S. C. Brown, Phys. Rev. **76**, 1697 (1949).
[5] F. J. Mehr and M. A. Biondi, Phys. Rev. **181**, 264 (1969).
[6] R. B. Bryan, R. B. Holt, and O. Oldenberg, Phys. Rev. **106**, 83 (1957).
[7] A. C. Faire, O. T. Fundingsland, A. L. Aden, and K. S. W. Champion, J. Appl. Phys. **29**, 928 (1958).
[8] A. C. Faire and K. S. W. Champion, Phys. Rev. **113**, 1 (1959).
[9] E. C. Zipf, Geophys. Res. Lett. **7**, 645, doi:10.1029/GL007i009p00645 (1980).
[10] J. L. Queffelec, B. R. Rowe, M. Morlais, J. C. Gomet, and F. Vallee, Planet. Space Sci. **33**, 263 (1985).
[11] A. Canosa, J. C. Gomet, B. R. Rowe, and J. L. Queffelec, J. Chem. Phys. **94**, 7159 (1991).
[12] M. Geoghegan, N. G. Adams, and D. Smith, J. Phys. B **24**, 2589 (1991).
[13] A. J. Cunningham and R. M. Hobson, J. Phys. B **5**, 2328 (1972).
[14] P. M. Mul and J. W. McGowan, J. Phys. B **12**, 1591 (1979).
[15] C. Noren, F. B. Yousif, and J. B. A. Mitchell, J. Chem. Soc., Faraday Trans. 2 **85**, 1697 (1989).
[16] D. Kella, P. J. Johnson, H. B. Pedersen, L. Vejby-Christensen, and L. H. Andersen, Phys. Rev. Lett. **77**, 2432 (1996).
[17] J. R. Petersen, A. Le Padellec, H. Danared, G. H. Dunn, M. Larsson, Å. Larson, R. Peverall, C. Strömholm, S. Rosén, M. af Ugglas, and W. J. van der Zande, J. Chem. Phys. **108**, 1978 (1998).
[18] M. R. Torr and D. G. Torr, Rev. Geophys. Space Phys. **20**, 91, doi:10.1029/RG020i001p00091 (1982).
[19] D. W. Rusch, A. I. Stewart, P. B. Hays, and J. H. Hoffman, J. Geophys. Res. **80**, 2300, doi:10.1029/JA080i016p02300 (1975).
[20] J. L. Fox and A. Hać, J. Geophys Res. E **102**, 9191, doi:10.1029/97JE00086 (1997).
[21] H. Lammer, W. Stumptner, G. J. Molina-Cuberos, S. J. Bauer, and T. Owen, Planet. Space Sci. **48**, 529 (2000).
[22] Y. L. Yung and J. R. Lyons, Geophys. Res. Lett. **17**, 1717, doi:10.1029/GL017i010p01717 (1990).
[23] S. L. Guberman, Geophys. Res. Lett. **18**, 1051, doi:10.1029/91GL01157 (1991).
[24] S. L. Guberman, J. Phys. Chem. **111**, 11254 (2007).
[25] S. L. Guberman, "Excited core states in the dissociative recombination of N_2^+," in *Dissociative Recombination: Theory, Experiment and Applications*, edited by W. J. van der Zande (Institute of Physics, Bristol, 2009), p. 012001.
[26] S. L. Guberman, "The dissociative recombination of N_2^+," in *Dissociative Recombination of Molecular Ions with Electrons*, edited by S. L. Guberman (Kluwer Academic/Plenum: New York, 2003), p. 187.
[27] D. R. Bates, Phys. Rev. **78**, 492 (1950).
[28] S. L. Guberman, Phys. Rev A **49**, R4277 (1994).
[29] S. L. Guberman, "Recent developments in dissociative recombination," in *Atomic Collisions: A Symposium in Honor of Christopher Bottcher (1945–1993)* (American Institute of Physics, New York, 1994), p. 88.
[30] J. N. Bardsley, J. Phys. B **1**, 365 (1968).
[31] T. F. O'Malley, J. Phys. B **14**, 1229 (1981).
[32] A. P. Hickman, J. Phys. B **20**, 2091 (1987).
[33] S. L. Guberman and A. Giusti-Suzor, J. Chem. Phys. **95**, 2602 (1991).
[34] S. L. Guberman, "Electron-ion continuum-continuum mixing in dissociative recombination," in *Dissociative Recombination: Theory, Experiment, and Applications*, edited by B. R. Rowe, J. B. A. Mitchell, and A. Canosa (Plenum, New York, 1993), p. 47.
[35] S. L. Guberman, "The role of Rydberg states in dissociative recombination," in *Dissociative Recombination: Theory, Experiment, and*

Applications, edited by D. Zajfman, J. B. A. Mitchell, B. Rowe, and D. Schwalm (World Scientific, Teaneck, 1996), p. 64.
[36]S. L. Guberman, "*Ab initio* studies of dissociative recombination," in *Dissociative Recombination: Theory, Experiment and Applications*, edited by J. B. A. Mitchell and S. L. Guberman (World Scientific, Teaneck, 1989), p. 45.
[37]S. L. Guberman, "New mechanisms for dissociative recombination," in *The Physics of Electronic and Atomic Collisions, XIX International Conference, Book of Invited Papers*, edited by L. J. Dube *et al.* (American Institute of Physics, New York, 1995), p. 307.
[38]Z. Amitay, D. Zajfman, P. Forck, T. Heupel, M. Grieser, D. Habs, R. Repnow, D. Schwalm, A. Wolf, and S. L. Guberman, Phys. Rev. A **53**, R644 (1996).
[39]S. L. Guberman, Science **278**, 1276 (1997).
[40]S. L. Guberman, "Isotope effects in dissociative recombination," in *Dissociative Recombination: Theory, Experiment, and Applications III*, edited by M. Larsson, J. B. A. Mitchell, and I. Schneider (World Scientific, Singapore, 2000), p. 111.
[41]D. Stahel, M. Leoni, and K. Dressler, J. Chem. Phys. **79**, 2541 (1983).
[42]S. K. Shih, W. Butscher, R. J. Buenker, and S. D. Peyerimhoff, Chem. Phys. **29**, 241 (1978).
[43]H. H. Michels, *Advances in Chemical Physics*, edited by I. Prigogine and S. Rice (Wiley-Interscience, New York, 1981), Vol. 45.
[44]J. Almlöf and P. R. Taylor, J. Chem. Phys. **86**, 4070 (1987).
[45]F. B. van Duijneveldt, Gaussian basis sets for the atoms H–Ne for use in molecular calculations, IBM Research Report RJ-945 (1971).
[46]P. E. M. Siegbahn, A. Heilberg, B. Roos, B. Levy, Phys. Scr. **21**, 323 (1980).
[47]P. E. M. Siegbahn, J. Chem. Phys. **72**, 1647 (1980).
[48]P. E. M. Siegbahn, C. W. Bauschlicher, B. Roos, P. R. Taylor, J. Almlöf, Molecule-Sweden.
[49]H.-J. Werner and P. J. Knowles, J. Chem. Phys. **82**, 5053 (1985).
[50]H.-J. Werner and P. J. Knowles, J. Chem. Phys. **89**, 5803 (1988).
[51]MOLPRO is a package of *ab initio* programs written by H.-J. Werner and P. J. Knowles, with contributions from R. D. Amos, A. Bernhardsson, A. Berning *et al.*, MOLPRO-2000.1.
[52]T. H. Dunning, Jr., J. Chem. Phys. **90**, 1007 (1989).
[53]S. L. Guberman, "Quantum yields in the dissociative recombination of N_2^+" (unpublished).
[54]J. W. Ledbetter, Jr. and K. Dressler, J. Mol. Spectrosc. **63**, 370 (1976).
[55]B. R. Lewis, S. T. Gibson, W. Zhang, H. Lefebvre-Brion, and J.-M. Robbe, J. Chem. Phys. **122**, 144302 (2005).
[56]B. R. Lewis, A. N. Heays, S. T. Gibson, H. Lefebvre-Brion, and R. Lefebvre, J. Chem. Phys. **129**, 164306 (2008).
[57]H. Lefebvre-Brion as reported in Ref. 54.
[58]M. Leoni and K. Dressler, J. Appl. Math. Phys. (ZAMP) **22**, 795 (1971).
[59]K. P. Huber and G. Herzberg, *Constants of Diatomic Molecules* (Van Nostrand Reinhold, New York, 1979).
[60]A. Lofthus and P. H. Krupenie, J. Phys. Chem. Ref. Data **6**, 113 (1977).
[61]J. P. Sprengers, E. Reinhold, W. Ubachs, K. G. H. Baldwin, and B. R. Lewis, J. Chem. Phys. **123**, 144315 (2005).
[62]D. Spelsburg and W. Meyer, J. Chem. Phys. **115**, 6438 (2001).
[63]In the prior discussion of the $2^1\Sigma_g^+$ state in Ref. 24, it was incorrectly stated that the cc-pVTZ basis set was used. The basis used was the [4s, 3p, 2d, 1f] as described in this paper.
[64]H. H. Michels, J. Chem. Phys. **53**, 841 (1970).
[65]W. C. Ermler, J. P. Clark, and R. S. Mulliken, J. Chem. Phys. **86**, 370 (1987).
[66]K. Kaufmann, W. Baumeister, and M. Jungen, J. Phys. B **22**, 2223 (1989).
[67]W. J. Hunt and W. A. Goddard III, Chem. Phys. Lett. **3**, 414 (1969).
[68]H. Feshbach, Ann. Phys. (NY) **5**, 357 (1958).
[69]A. U. Hazi, "Molecular resonance phenomena," in *Electron-Atom and Electron-Molecule Collisions*, edited by J. Hinze (Plenum, New York, 1983), p. 103.
[70]H. Lefevbre-Brion and C. M. Moser, J. Chem. Phys. **43**, 1394 (1965).
[71]P. Cremaschi, A. Chattopadhyay, P. V. Madhavan, and J. L. Whitten, Chem. Phys. **109**, 117 (1986).
[72]A. Giusti, J. Phys. B **13**, 3867 (1980).
[73]M. J. Seaton, Rep. Prog. Phys. **46**, 167 (1983).
[74]U. Fano, Phys. Rev. **124**, 1866 (1961).
[75]H. Helm and P. C. Cosby, Phys. Rev. A **38**, 115 (1988).
[76]S. L. Guberman, "Dissociative recombination of vibrationally excited N_2^+" (unpublished).
[77]H. H. Michels, Theoretical Determination of Electronic Transition Probabilities for Diatomic Molecules, AFWL-TR-72-1, May, 1972.
[78]M. R. Mahdavi, J. B. Hasted, and M. M. Nakshbandi, J. Phys. B **4**, 1726 (1971).
[79]P. M. Mul and J. W. McGowan, J. Phys. B **12**, 1591 (1979).
[80]J. B. A. Mitchell, Phys. Rep. **186**, 215 (1990).
[81]A. I. Florescu-Mitchell and J. B. A. Mitchell, Phys. Rep. **430**, 277 (2006).
[82]D. R. Bates and J. B. A. Mitchell, Planet. Space Sci. **39**, 1297 (1991).
[83]C. H. Sheehan and J.-P. St.-Maurice, J. Geophys. Res. **109**, A03302, doi:10.1029/2003JA010132 (2004).
[84]R. Johnsen, Int. J. Mass Spectrom. Ion Process **81**, 67 (1987).
[85]R. Johnsen, ~~"Comments on developments in the theory of dissociative recombination over the past 60 years,"~~ in *Dissociative Recombination: Theory, Experiment and Applications*, edited by S. L. Guberman and A. E. Orel (Institute of Physics, Bristol, 2011), p. 012002.

DR Experiments in the 60 years since the Bates paper